university of groningen / faculty of mathematics and natural sciences / kapteyn astronomical institute

THz Beam Modulation By Optical Illumination of a Semiconductor Substrate

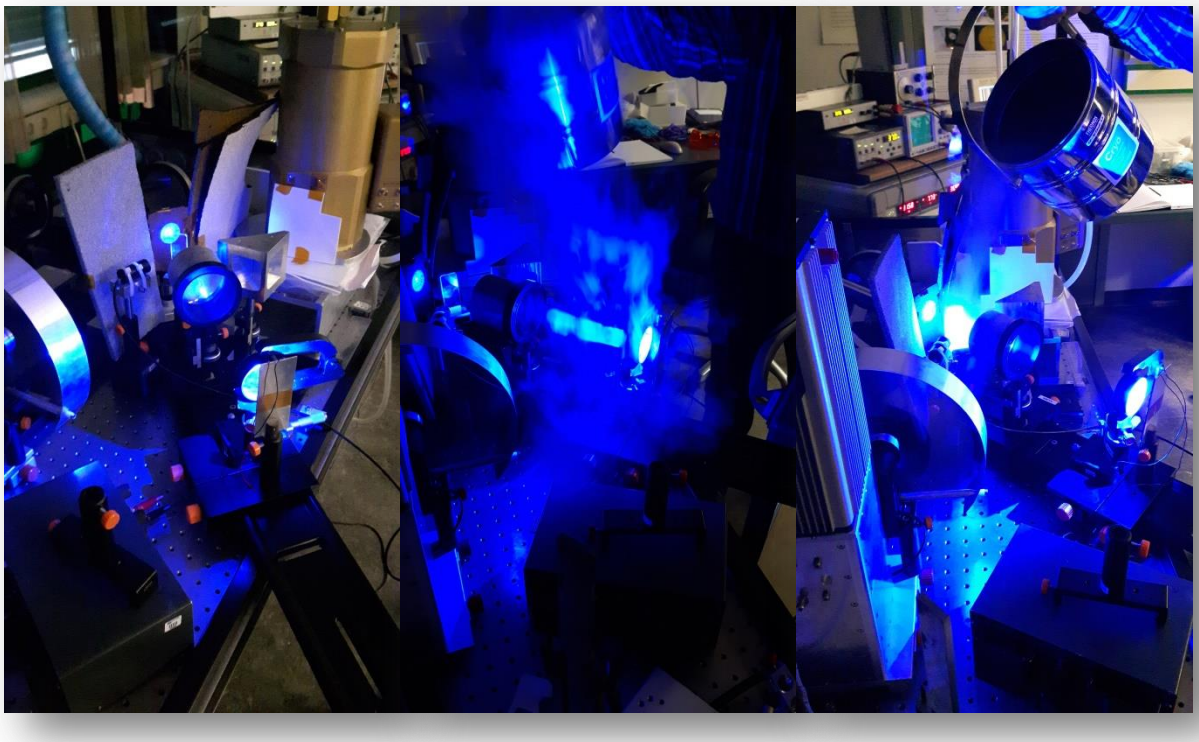

Ing. Tim Ketelaar

Master's thesis Instrumentation and Informatics

Supervisor:

Prof. Dr. Andrey Baryshev (NOVA)

Second Reader:

Dr. ir. W. Jellema (SRON)

Coordinator:

Prof. Dr. M.A.W. Verheijen (Kapteyn Institute)

06/07/2018

‘Finding the right Green’s function is not much more difficult than feeding mustard to a cat´

Russian problem solving

´I believe that we can ´sense´ the future, although it´s not clear in physics why you can´t see it`

Brian Josephson

Abstract

For the instrumentation development of the Atacama Large Millimeter Array (ALMA) located in Chili, we consider the modulation of submm/THz radiation by utilising properties of semiconductor materials. In essence, a semiconductor substrate is illuminated with different light sources, modifying the semiconductor properties. Exactly these properties are of interest which alter the propagation of THz radiation. In particular, a high-resistivity slab of silicon (Si) has been used. The first experiment involves a calibration which relates the intensity of THz radiation to the intensity of optical illumination. The dependence turned out to be a modified inverse power law. In the second experiment we go into detail on the spectral properties of absorption in the Si substrate using the Fourier Transform Spectrometer (FTS) setup. A frequency dependence of the THz transmission was found, which is in favour of the local oscillators used in ALMA. Subsequently, measurements were performed with a heterodyne receiver system. In this experiment, investigations have been made regarding the noise temperature contributions of THz modulation due to the Si substrate. As was consistent for all light sources, the additional noise temperature is within the noise of the measurement. In addition, measurements have been carried out to study the phase noise contributions at different frequency offsets from the central carrier wave. Up to the spectral resolution of ALMA ($100\ KHz$) there is no significant contribution in terms of phase noise power. Consequently, the method of optical illumination of a semiconductor substrate to modulate THz radiation as presented in this thesis is deemed suitable for use in a low noise heterodyne system.

Acknowledgements

First of all, I would like to thank Andrey Baryshev for his good supervision that was provided during my research and for guiding me through any obstacles I faced. I want to thank Andrey Khudchenko for being the helping hand during serendipitous experiments and for sharing his marvellous anecdotes. Finally, I want to thank Kirill Rudakov for taking time to give critical feedback and also for sharing his insightful ideas. It was just simply '*Amazing*'.

Contents

1. Introduction

The work as presented in this master's thesis is related to the Atacama Large Millimeter Array (ALMA) located in Chili. Specifically, the work is concerned with the modulation of submm/THz radiation by means of optical illumination of a high-resistivity Si substrate. This poses a variety of challenges both experimentally as well as theoretically. In essence, the Si substrate is illuminated with a high-power light source, exciting charged (quasi)-particles such as electrons into the conduction band (CB) where the properties of the semiconductor are modified. In general, the Si substrate is largely transparent to THz radiation with small losses. However, since an electron plasma will form inside the Si substrate part of the THz radiation will be reflected additionally. Moreover, the electrons will diffuse into the Si substrate leading to interactions with the semiconductor material such as electron-phonon scattering (Gallacher, 2012) . Consequently, the propagation of THz radiation will be altered and several transmission (resonance) peaks will be visible. In order to acquire a basic understanding of these phenomena, first a theoretical study will be carried out to model the propagation of a THz beam through a Si substrate. Subsequently, calibration measurements will be considered as to how optical illumination of the Si substrate behaves in relation to the intensity of the THz beam. This can be performed with a standard Fourier Transform Spectrometer (FTS) setup. Subsequently, the FTS can be extended to study the interference patterns (i.e. interferograms) related to intrinsic properties of the Si substrate such as the relative permittivity as well as observing the transmission behaviour at various THz frequencies. In order to study the system noise temperature characteristics, the heterodyne receiver setup will be used. The setup includes a Local Oscillator (LO) operating in the frequency range of $600 - 750\ GHz$ together with a hot-cold source. The LO is used in conjunction with a Superconductor-Insulator-Superconductor (SIS) mixer generating a spectrum of Intermediate Frequency (IF) signals i.e. $|f_1 - f_2|$. By replacing the hot-cold source with another LO, the heterodyne receiver setup will be used to investigate whether optical illumination of the Si substrate contributes to the phase noise power at different frequency offsets from the central carrier wave. This will be the final method to conclude whether THz modulation using a semiconductor material is feasible for a low noise heterodyne system. Therefore, the results will be a probe as to whether modulation of THz radiation can be achieved effectively considering the use of semiconductor materials in the phased array feeds of ALMA.

2. Background Theory

2.1 Free-carrier Dynamics

In this section, the theoretical analysis will be carried out related to free-carrier dynamics inside a semiconductor material. This analysis is required in order to get an understanding of how a THz beam propagates through an optically illuminated semiconductor material. Hence, the goal is to compute the transmission of the THz beam as a function of optical illumination using various light sources. Specifically, a high-resistivity undoped silicon (Si) substrate will be considered having a certain thickness h. In general, the Si substrate is transparent to THz radiation whilst having a low insertion loss (Benford, et al., 1998). As soon as the Si substrate is illuminated, a distribution of charge carriers i.e. electron-hole pairs will be formed with a generation rate g and a carrier life time τ_e that interacts with the THz radiation. The carrier generation rate is reduced exponentially in the z-direction defined by (Kannegulla, 2015) (University of Reading):

$$\boldsymbol{g(z) = \alpha P_0 (1 - R) e^{-\alpha z / h\nu}} \,. \tag{1}$$

$$\boldsymbol{\alpha = \frac{4\pi\kappa}{\lambda_{opt}}} \,. \tag{2}$$

Here, α is the absorption coefficient defined in terms of the extinction κ and the optical wavelength λ_{opt}. Moreover, $h\nu$ corresponds to the photon energy of optical illumination and P_0 is the corresponding power density. Subsequently, the reflectivity of the Si substrate can be defined assuming normal incidence and a refractive index of air $n_0 \approx 1$ (Palik, 1988):

$$\boldsymbol{\left|\frac{1-\tilde{n}_s}{1+\tilde{n}_s}\right|^2} \,. \tag{3}$$

Here, $\tilde{n}_s = n_s + i\kappa_s$ is the complex refractive index of the Si substrate. The complex refractive index $\tilde{n}_s(x,z)$ will be computed and is related to the carrier concentration N_e. Note that a two-dimensional approach will be used, which will ultimately be reduced to a one-dimensional case under specific conditions (detailed later on). The one- and two-dimensional approach are applicable to analytically study the effect of the optical illumination area with respect to the THz modulation performance. Nevertheless, three-dimensional numerical solutions to the photo-excited carrier distributions exist also in order to study the spatial resolution of THz modulation (Kannegulla, 2015). Hence, in order to analytically evaluate the theory in question, the one- and two-dimensional approach will be elaborated. In order to do so, a continuity equation needs to be solved which yields the carrier concentration distribution as well as a so called Lorentz-Drude model (Ulbricht, et al., 2011). Essentially, this model relates the carrier concentration to the complex permittivity of the Si substrate. According to the conservation of charge (i.e. charge is neither created nor destroyed), the optically induced carrier concentration $N_e(x,z,t)$ can be described by the following continuity equation (Kannegulla, 2015):

$$\boldsymbol{\frac{\partial N_e}{\partial t} = D_{eff} \nabla^2 N_e - \frac{N_e}{\tau_e} + g} \,. \tag{4}$$

$$\boldsymbol{\nabla^2 = \frac{\partial^2}{\partial x^2} + \frac{\partial^2}{\partial z^2}} \,. \tag{5}$$

Here, τ_e is the carrier lifetime and D_{eff} is the effective carrier diffusion coefficient. The diffusion coefficient is a function of the effective carrier mobility μ_{eff} contributed by both the electrons and holes i.e. (Kannegulla, 2015):

$$\boldsymbol{D_{eff} = \frac{2\mu_{eff}kT}{q}} \ . \tag{6}$$

$$\boldsymbol{\mu_{eff} = \frac{1}{1/\mu_e + 1/\mu_h}} . \tag{7}$$

Here, μ_e and μ_h is the electron/hole mobility respectively. The carriers are induced by absorption of the incoming photons in an area of width w and subsequently diffuses over the Si substrate of thickness h. An important assumption will be made which leads to the boundary conditions of the solution for the continuity equation. The surface recombination is assumed to be negligible so that at $z = 0$ and $z = h$ the change in carrier concentration is unaltered i.e. $\partial_z n(x,z)|_{z=0} = 0$ and $\partial_z n(x,z)|_{z=h} = 0$ (Kannegulla, 2015). Hence, taking into account these boundary conditions the two-dimensional steady-state solution of the continuity equation can be defined as follows (Kannegulla, 2015):

$$\boldsymbol{N_e^{2D}(x,z) = \int_0^h \int_{\frac{-w}{2}}^{\frac{w}{2}} \frac{g(\eta)}{D_{eff}} G(x,z,\xi,\eta) d\xi d\eta} \ . \tag{8}$$

Here, $G(x,z,\xi,\eta)$is the Green's function (Parnell, 2013) and $g(\eta)$ is the generation rate as defined previously. The Green's function is defined in terms of the modified Bessel function of the second kind K_0 and is a function of the plane parameters η (plasma), ξ (substrate) as well as the carrier diffusion length $L_D = \sqrt{\tau_e D_{eff}}$ (Kannegulla, 2015). A detailed definition for the Green's function can be found in Appendix A.

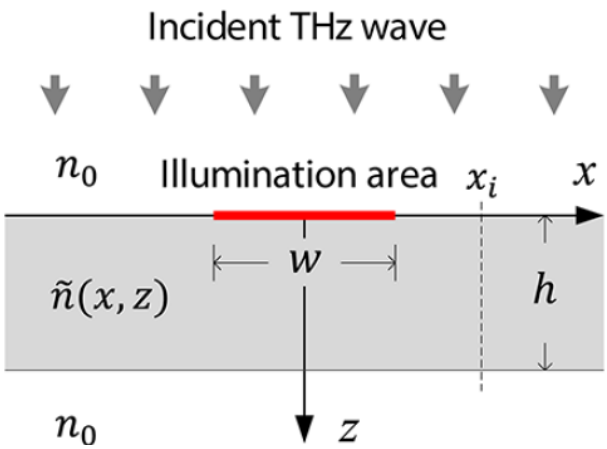

Figure 1: Schematic overview of the model in case of optical illumination of a Si substrate. (Kannegulla, 2015)

Subsequently, applying a flood exposure condition i.e. $w \to \infty$ and assuming a small carrier life time implying a small diffusion length ($L_D \ll h$) the solution can be defined for a one-dimensional system (Kannegulla, 2015):

$$N_e^{1D}(z)\Big|_{L_D \ll h} = \frac{\tau_e \alpha P_0 (1-R)}{h\nu} \frac{1}{1-(\alpha L_D)^2} \left(e^{-\alpha z} - \alpha L_D e^{-z/L_D}\right) \ . \tag{9}$$

Since flood exposure of the Si substrate entails a homogeneous illumination and for small diffusion lengths the carrier concentration is isotropic the one-dimensional result is validated. Consequently, this equation describes the one-dimensional carrier concentration induced by optical illumination of the Si substrate. In order to relate the carrier concentration to the complex permittivity ($\tilde{\varepsilon}_D = \varepsilon_{re} + i\varepsilon_{im}$) the total carrier concentration will be considered i.e. $N_s = N_e + N_i$, where N_i is the intrinsic carrier concentration. This relation is consistent throughout the Si substrate according to the Lorentz-Drude model (Ulbricht, et al., 2011):

$$\varepsilon_{re}(x, z, \omega) = -\frac{N_s q^2 \omega^2}{m_e(\omega^4 + \omega^2 \gamma_e^2)\varepsilon_0} - \frac{N_s q^2 \omega^2}{m_h(\omega^4 + \omega^2 \gamma_h^2)\varepsilon_0} + \varepsilon_\infty . \tag{10}$$

$$\varepsilon_{im}(x, z, \omega) = \frac{N_s q^2 \omega \gamma_e}{m_e(\omega^4 + \omega^2 \gamma_e^2)\varepsilon_0} + \frac{N_s q^2 \omega \gamma_h}{m_h(\omega^4 + \omega^2 \gamma_h^2)\varepsilon_0} . \tag{11}$$

Here, $\omega = 2\pi\nu$ is the frequency of THz radiation, ε_∞ is the absolute permittivity of the Si substrate, ε_0 is the vacuum permittivity, $m_{e,h}$ and $\gamma_{e,h}$are the effective masses/damping coefficients of the electron and hole respectively. Subsequently, the real and imaginary parts of the complex refractive index can be computed according to definitions of the permittivity as defined in equations 10 and 11. Therefore (Kannegulla, 2015):

$$n(x, z, \omega) = \sqrt{\left(\varepsilon_{re} + \sqrt{\epsilon_{re}^2 + \varepsilon_{im}^2}\right)/2} \ . \tag{12}$$

$$\kappa(x, z, \omega) = \sqrt{\left(-\varepsilon_{re} + \sqrt{\epsilon_{re}^2 + \varepsilon_{im}^2}\right)/2} \ . \tag{13}$$

2.2 THz Transmission

Now that the complex refractive index has been defined, one can compute the transmission of the THz beam according to a Fresnel transfer matrix technique (Born, et al., 1999). This technique takes into account a graded refractive index of the Si substrate (see figure 2). In essence, the Si substrate is defined in terms of m isotropic and homogeneous layers of thickness $\delta = 1\ \mu m \ll L_D$ and refractive indices $\tilde{n}_j = \tilde{n}(z = jh/m)$ for the jth layer. Then, the transmission can be computed via the following 2×2 scattering matrix (Kannegulla, 2015) (Jarry, et al., 2008):

$$S = \begin{pmatrix} S_{11} & S_{12} \\ S_{21} & S_{22} \end{pmatrix} = I_{01} \prod_{j=1}^{m} L_j I_{j(j+1)} \ . \tag{14}$$

Here, $I_{j(j+1)}$ is the transfer matrix comprising the wave propagation at the interface between the layers j and $j+1$ (Kannegulla, 2015):

$$I_{j(j+1)} = \frac{1}{t_{j(j+1)}} \begin{pmatrix} 1 & r_{j(j+1)} \\ r_{j(j+1)} & 1 \end{pmatrix} \ . \tag{15}$$

Here, $t_{j(j+1)} = 2\tilde{n}_j/(\tilde{n}_{j+1} + \tilde{n}_j)$ and $r_{j(j+1)} = (\tilde{n}_{j+1} - \tilde{n}_j)/(\tilde{n}_{j+1} + \tilde{n}_j)$ are the Fresnel coefficients at the $j(j+1)$ interface for a zero-order propagation. $\boldsymbol{I}_{01}$ describes the wave propagation at the very first interface i.e. the air-layer interface. Subsequently, the transfer matrix $\boldsymbol{L}_j$ can be described as follows (Kannegulla, 2015):

$$\boldsymbol{L}_j = \begin{pmatrix} e^{i\varphi_j} & 0 \\ 0 & e^{-i\varphi_j} \end{pmatrix}. \tag{16}$$

Here, $\varphi_j = 2\pi\delta\tilde{n}_j/\lambda_T$ is the phase shift of the THz beam with wavelength λ_T propagating through the jth layer with thickness δ and corresponding refractive index $\tilde{n}_j$. Finally, the transmission of the THz beam can therefore be derived by applying the definitions of equations 15 and 16 into equation 14 which made up the 2×2 scattering matrix (Kannegulla, 2015) (Dunleavy):

$$T = \left|\frac{1}{S_{11}}\right|^2. \tag{17}$$

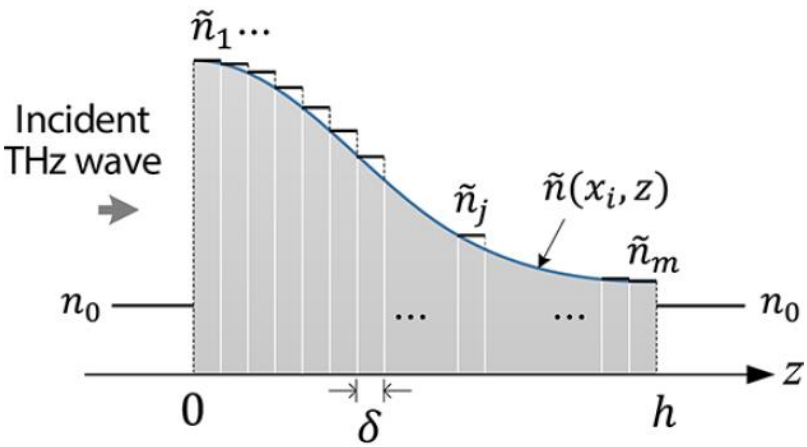

Figure 2: Discretised refractive index profile for THz transmission computation using the Fresnel transfer matrix method. (Kannegulla, 2015)

3. Light Source Calibration

3.1 Photodiode Calibration

Several light sources have been investigated as to which light source produces the highest irradiance on the Si substrate. More specifically, in order to get a desirable attenuation of the THz beam (at least -10 dB or higher) in turned out that intensities are required in the order of $1\ W/m^2$ or higher (Jiang et al., 2017). This is important as a considerable attenuation of the THz beam is required in order to perform noise temperature measurements. At first, three different high power LEDs were examined namely a deep red, green and a royal blue LED. See figure 3 for the spectral details.

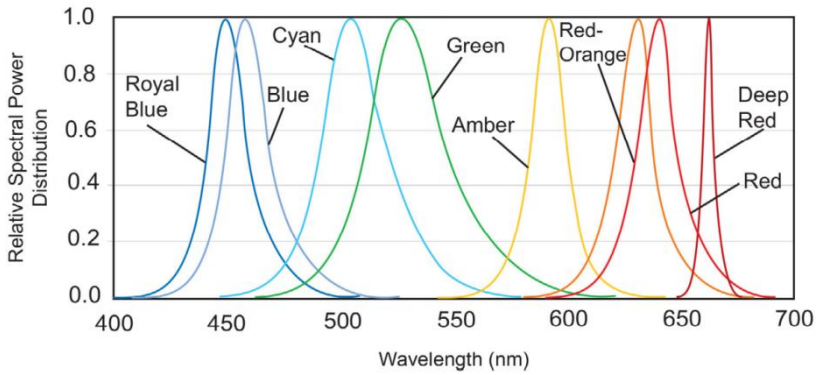

Figure 3: Spectral power versus wavelength of several LEDs. Royal blue, green and deep red have been incorporated in the experimental setup (Lumileds, 2017).

The first important aspect to take into account for calibration of the photodiode is the spectral sensitivity curve depicted in figure 4. As can be observed, the spectral sensitivity peaks in green around $550\ nm$. Consequently, the peak wavelengths (minimum/maximum) of the green, deep red and royal blue LEDs are $520/540\ nm$, $650/670\ nm$ and $440/460\ nm$ respectively. Hence, the spectral sensitivity for the green LED at $530\ nm$ is $S_\lambda = 0.95$, $S_\lambda = 0.65$ for the red LED at $660\ nm$ and $S_\lambda = 0.7$ for the blue LED at $450\ nm$. These sensitivity values should be taken into account for making a proper comparison between the three LEDs involved in the experiments to be carried out.

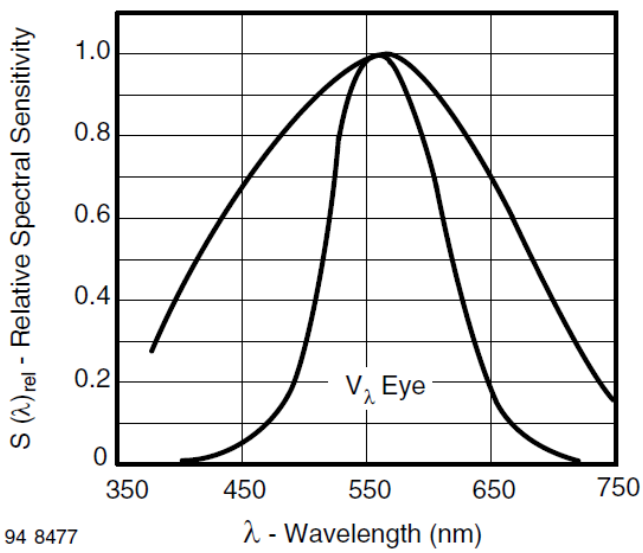

Figure 4: Spectral sensitivity curve of the Si photodiode (Vishay, February 2017)

Another important graph specifying the photodiode characteristics is depicted in figure 5, which relates the short circuit current to the illuminance. The relation is depicted on a log-log scale which corresponds to a certain power law dependence at least up to $1\ mA$. In this manner, a computation can be made as to the amount of power that will be received from the light source onto the photodiode per square centimetre (W/cm^2). This computation will be carried out for all light sources involved in the experiment by using the definition of lux and by considering several assumptions.

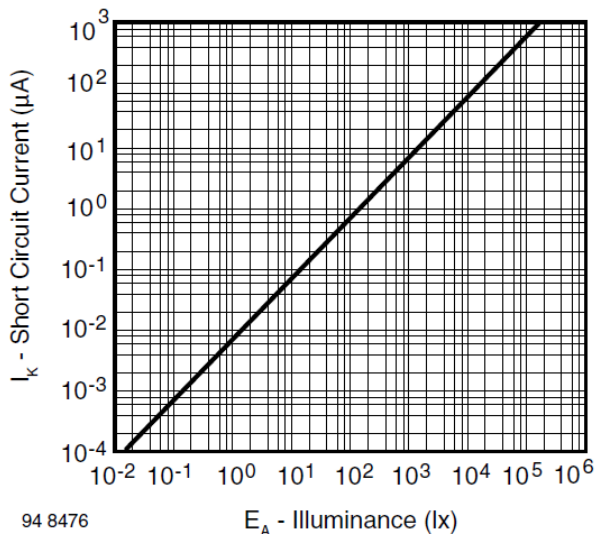

Figure 5: Photodiode short circuit current $[\mu A]$ vs illuminance $[lx]$ (Vishay, February 2017).

The setup configuration comprises the light source (LED), a hyperbolic lens ($f \approx 3\ cm$) as well as the silicon-based photodiode. The setup has been schematically illustrated in figure 6. Subsequently, the data was acquired using an input current ranging from 0 to $1A$ in discrete steps of $100mA$. The results are presented in table 1.

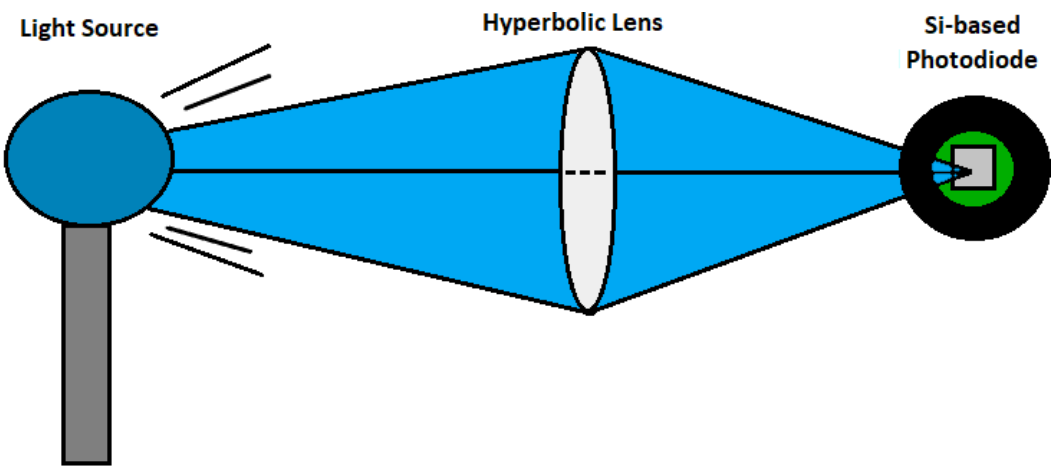

Figure 6: Optical scheme for light source calibration using a Si-based photodiode

Input Current $[mA]$	Red LED Photodiode Current $[mA]$	Green LED Photodiode Current $[mA]$	Blue LED Photodiode Current $[mA]$
100	0.43	0.73	1.81
200	0.8	1.25	3.22
300	1.15	1.65	4.48
400	1.5	2.00	5.67
500	1.81	2.32	6.73
600	2.09	2.56	7.71
700	2.38	2.89	8.56
800	2.63	3.10	9.59
900	2.88	3.28	10.31
1000 irradiance $[mW/cm^2]$	3.10 (28)	3.45 (31)	11.15 (100)

Table 1: Photodiode reading for three different LEDs in terms of varying input current together with the irradiance at the highest input current denoted in brackets.

Note that in this experiment, two blue LEDs were mounted together in series whereas in case of red and green only one LED was used. This clarifies the larger difference between the readings. Regardless, the blue LED seemed to yield the highest photodiode current and the red LED turned out to yield the lowest photodiode current. Subsequently, a computation can be made to define the amount of power that is received by the photodiode per square centimetre i.e. the irradiance. This is done by extrapolating the graph in figure 5 under the assumption that it remains linear on the log-log scale. Essentially, one lux is defined as one lumen per square metre. Lumen is the luminous flux of light produced by a source emitting one candela per steradian. Successively, one candela is the luminous intensity (i.e. wavelength-weighted power) of a source of $540\ THz$ with a radiant intensity of $\frac{1}{683} W/sr$ (NIST, 1979). In case of an LED, the radiation profile is Lambertian which implies a solid angle of approximately $2\pi\ ster$. However, the hyperbolic lens only captures a fraction of this light to be focussed on the photodiode. Therefore, the solid angle becomes:

$$\Omega = \frac{\boldsymbol{A}}{\boldsymbol{r^2}} = 2.185 \times 10^{-3} m^2 / 0.06^2 m^2 \approx 0.61\ sr\ .$$

Performing the computation for the blue LED leads to the following:

$$11.15\ mA = 1.115 \times 10^6\ \ lumen/m^2 = 111.5\ \ lumen/cm^2,$$

$$\text{where } 1\ mA = 1 \times 10^5\ \ lumen/m^2.$$

$$111.5\ lumen/cm^2 \times \frac{1}{683} W/sr \times 0.61\ sr \approx\ 100\ mW/cm^2,$$

$$\text{where } 1\ lumen = \frac{1}{683} W/sr\ .$$

In case of the red and green LEDs, the photodiode currents of $3.10\ mA$ and $3.45\ mA$ correspond to an irradiance of $28\ \ mW/cm^2$ and $31\ \ mW/cm^2$ respectively.

3.2 Calibration Curves

3.2.1 Blue LED

With a similar optical scheme as depicted in figure 6, the photodiode could be calibrated in the general FTS setup (Weisstein, 2007). Essentially, the photodiode was positioned slightly above the $10\ mm$ aperture so that a real-time measurement could be performed. Hence, the area of illumination was slightly larger than the aperture as well, which resulted in a slightly lower irradiance of the Si substrate. A schematic overview of the new setup can be found in figure 7 below.

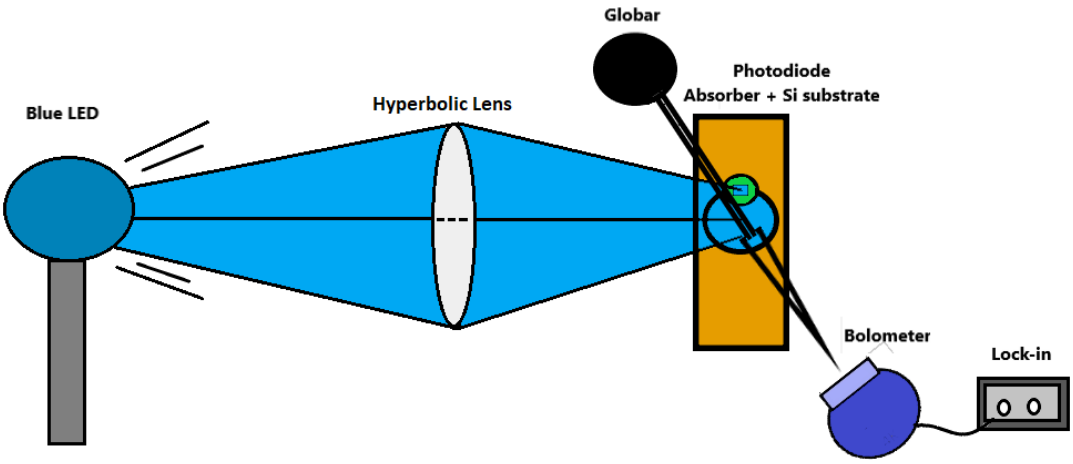

Figure 7: Optical scheme as used for calibration of the blue LED.

The curve as illustrated in figure 8 reveals the relation between Lock-in voltage versus photodiode current. As can be observed, there is some decrease in Lock-in voltage visible however it is too small to justify the kind of relation present. Hence, a larger attenuation of the THz beam is required to make a good statement about the type of dependence of the curve. Nonetheless, in the low attenuation regime the dependence looks rather linear. Consequently, a similar measurement with a microscope light (i.e. a high power halogen lamp connected to an optical fibre) has been carried out to illustrate the attenuation profile more accurately over a larger range.

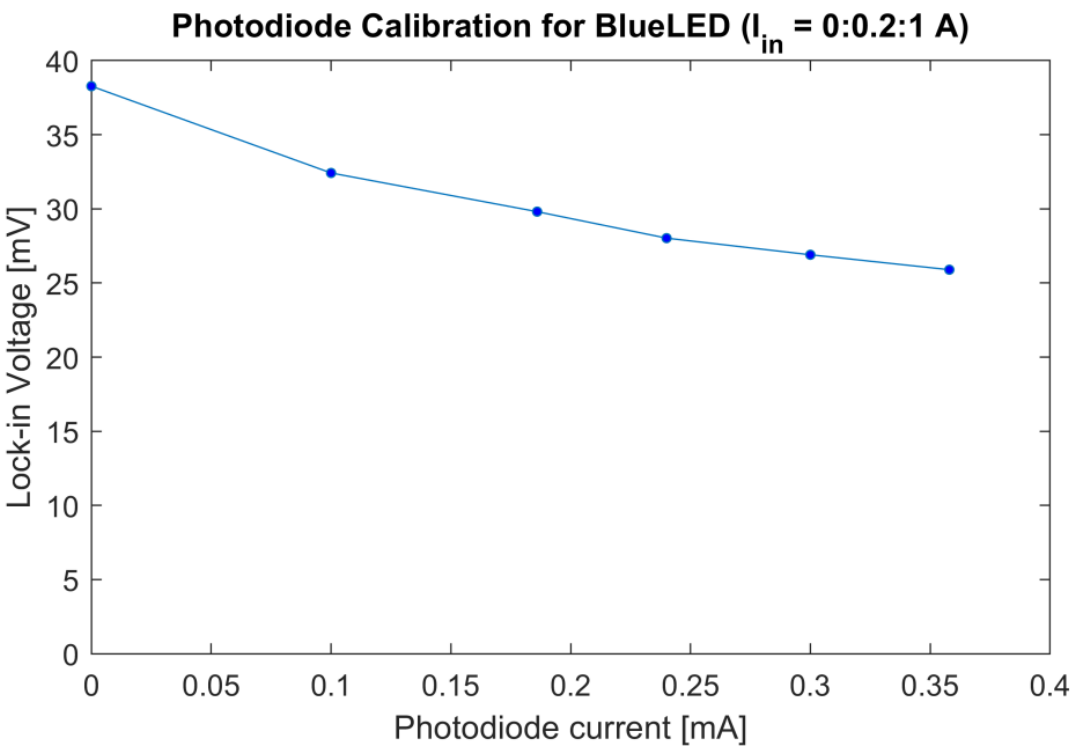

Figure 8: Calibration curve for the Si-based photodiode measured with a blue LED. The input current ranges from 0 to 1A in steps of 0.2A (i.e. six data points).

3.2.2 Microscope Light

Essentially, two separate measurements were carried out in order to arrive at the calibration curve using the microscope light. The microscope light is a white light source (halogen lamp) connected by an optical fibre having multiple illumination modes. First of all, a measurement was performed by means of illuminating the Si substrate in the FTS setup by moving the optical fibre backwards at fixed distance intervals. See figure 9 below for an overview of the optical setup.

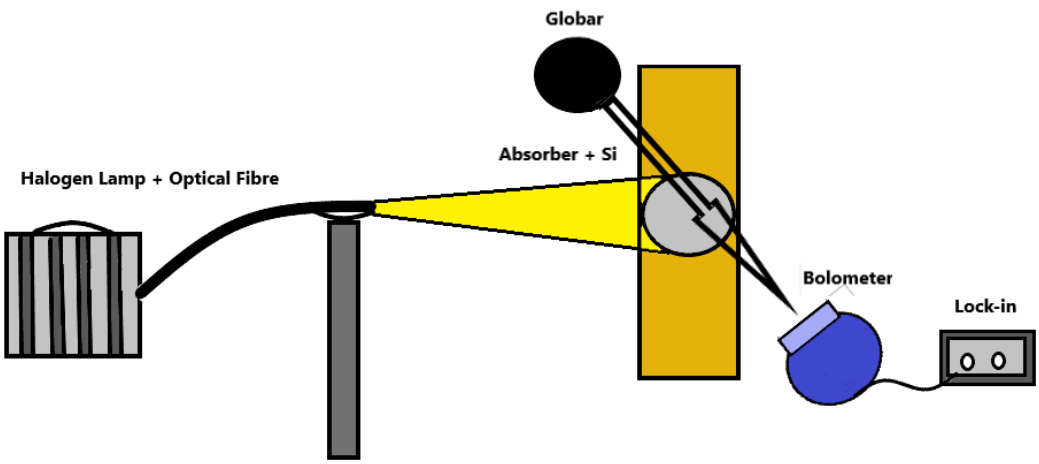

Figure 9: Schematic overview of the optical setup in case of the microscope light (halogen lamp with optical fibre).

The optical fibre is moved backwards from zero to six centimetres in steps of one centimetre (i.e. eight data points). Zero centimetres essentially is the closest position possible to the Si substrate without obscuring the THz beam. Since modifying the illumination mode of the light source changed the colour of light it was more convenient to carry out the measurement in this manner. This implies a curve depicting the relation between Lock-in voltage versus distance from the Si substrate, which turned out to be rather linear (see figure 10). The second measurement is performed with the photodiode which implies a curve depicting the relation between photodiode current and distance from the photodiode, which seemed to follow an inverse power law (see figure 11).

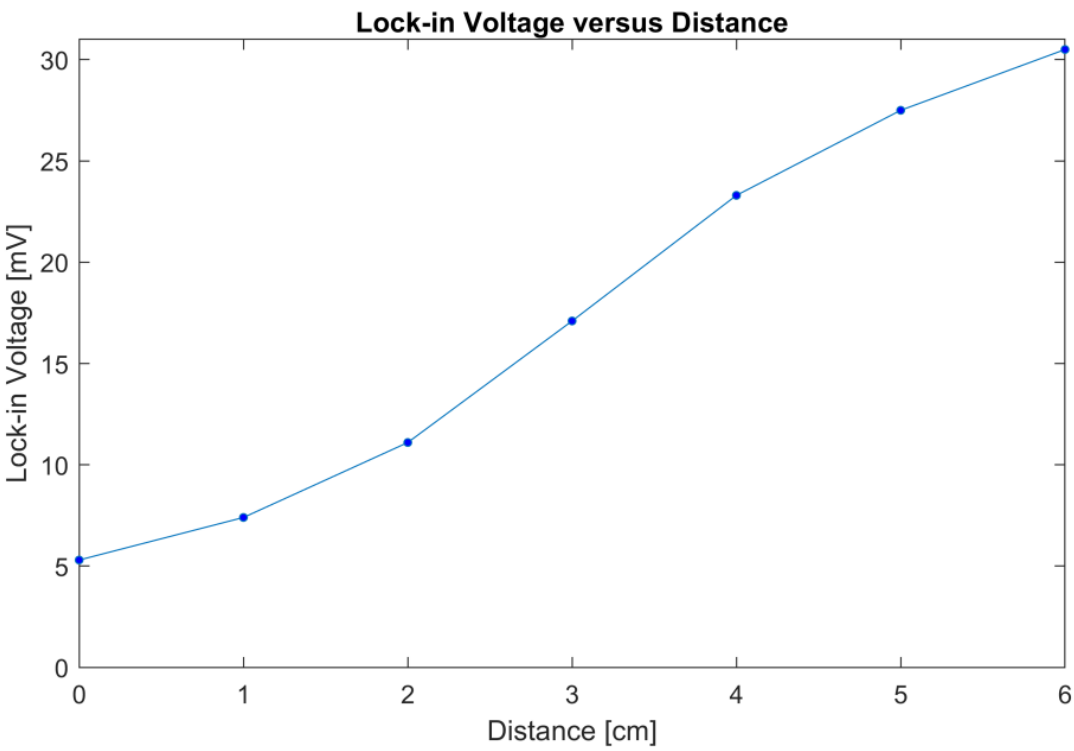

Figure 10: Relation between the Lock-in signal of the globar used in the FTS setup versus distance from the Si substrate using the microscope light (halogen lamp with optical fibre).

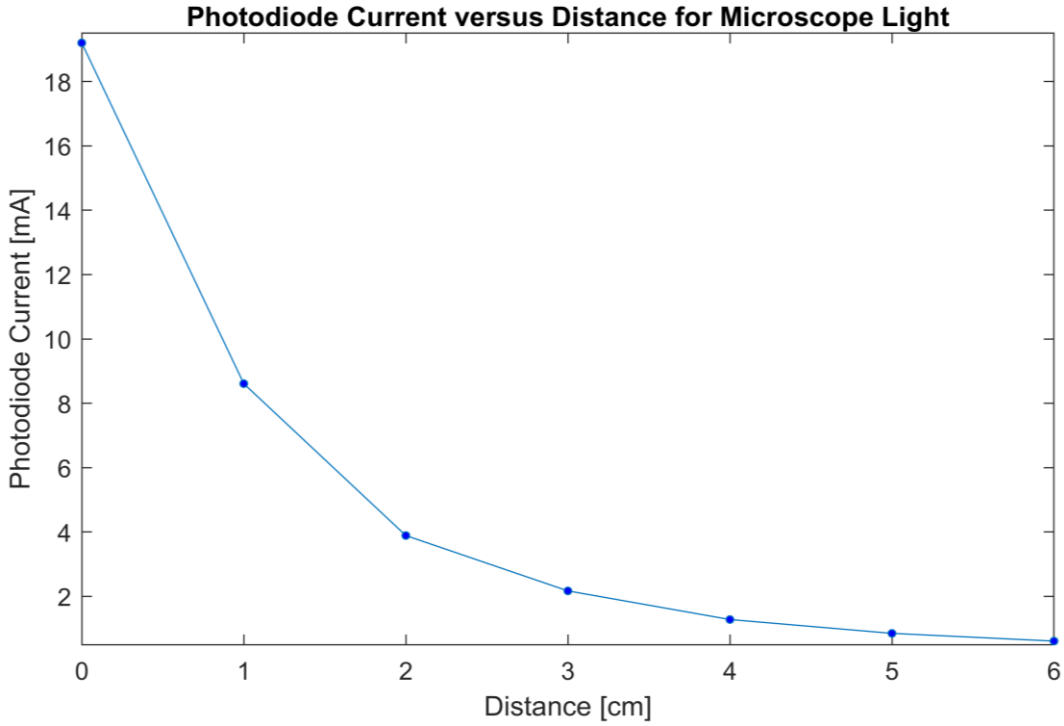

Figure 11: Relation between photodiode current and distance from the photodiode using the microscope light.

The combination of these two curves resulted in a curve depicting the relation between Lock-in voltage versus photodiode current as shown in figure 12. The result seems to follow a modified inverse power law i.e. an inverse power law with a modified slope. This relation is very significant as it specifies the connection between intensity of light on the Si substrate with the power of the THz beam. The high resistivity silicon becomes conductive and hence part of the THz beam is absorbed according to the electron/hole distribution in the silicon.

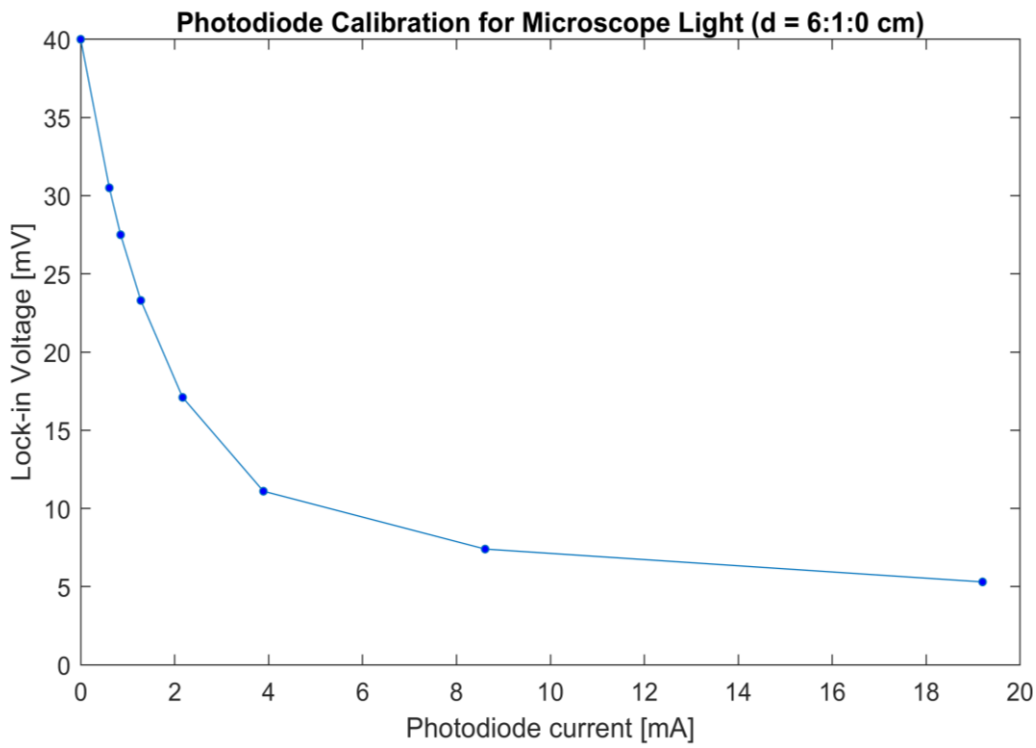

Figure 12: Photodiode calibration curve in case of a white light source (microscope light) connected by an optical fibre. This graph is the combined result of the graphs in figure 10 and 11.

4. FTS Experiment

4.1 Fourier Transform Spectrometer

In this experiment, the behaviour of THz radiation on a slab of high resistivity silicon is studied by means of a Fourier Transform Spectrometer (FTS) which is based upon interferometry (Hecht, 2017). In essence, an interferometer uses the superposition principle of waves having the same frequency (e.g. THz radiation). When two waves of frequency ω are combined, the amplitude is solely dependent on the phase difference between the two waves (Liu, 2012) (Thorne, 1988):

$$\boldsymbol{E_T} = \boldsymbol{E_1 e^{i\omega t}} + \boldsymbol{E_2 e^{i\omega t + \theta}} \,. \tag{18}$$

Hence, the waves will either undergo constructive (in-phase) or destructive (out-of-phase) interference. The interferometer used in the experiment is named a Michelson interferometer, which is based upon the phenomenon of amplitude splitting. Together with a translating or movable mirror this is named FTS. See figure 13 for an illustrative overview of the optical scheme as used in the experiment.

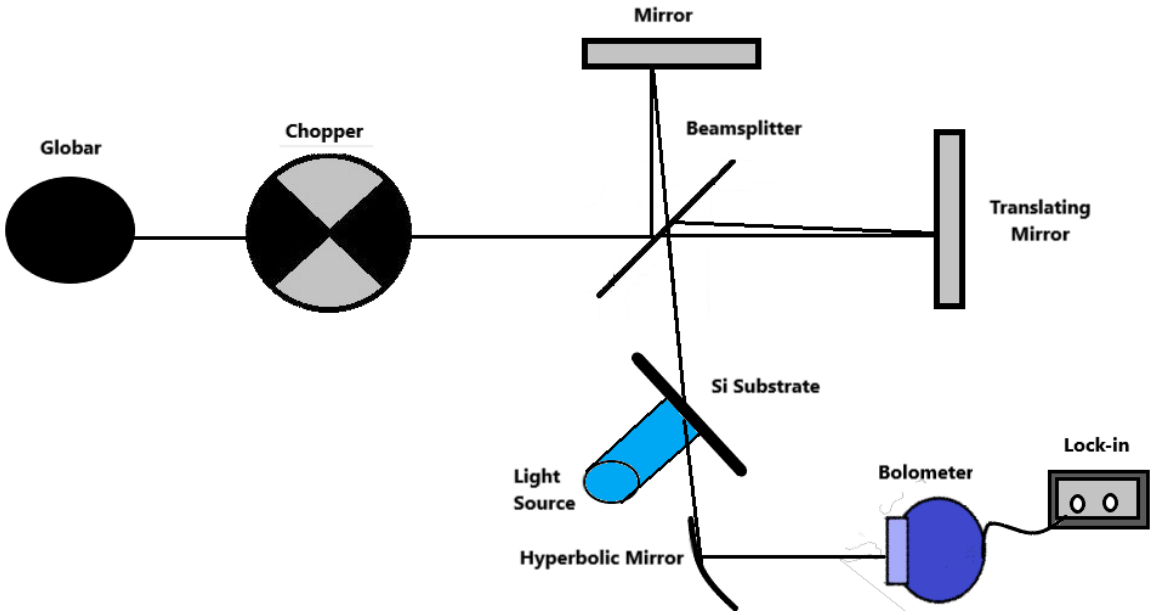

Figure 13: Optical scheme in case of the FTS experiment. The interferometer is based upon amplitude splitting named a Michelson interferometer.

Subsequently, the phase difference is dependent on the optical path difference between the two beams and is given as follows (Liu, 2012) (Thorne, 1988):

$$\boldsymbol{\theta} = \frac{2\pi}{\lambda}\Delta = \boldsymbol{2\pi\sigma}\Delta \,. \tag{19}$$

Here, σ is the wavenumber and Δ is the optical path difference or retardation. Then, the amplitude of the interference beam becomes (Liu, 2012) (Thorne, 1988):

$$\boldsymbol{E_T = E_0(e^{i\omega t} + e^{i\omega t + 2\pi\sigma\Delta})}\,. \tag{20}$$

Note that the assumption of equal splitting is assumed here i.e. $E_1 = E_2 = E_0$. Next, the intensity of the interference beam can be computed (Liu, 2012) (Thorne, 1988):

$$\boldsymbol{I}(\Delta) = \boldsymbol{|E_T E_t^*| = \tfrac{1}{2} I_0[1 + \cos(2\pi\sigma\Delta)]}\,. \tag{21}$$

This solution holds true for a monochromatic light source. If there is no optical path difference ($\Delta = 0$), the intensity is simply I_0. So the only variable that plays a significant role is Δ, which can be accurately controlled by the movable mirror. Therefore, by scanning the movable mirror over a certain distance, an interference pattern will be produced which is related to the spectrum of the source. In essence, the intensity as function of retardation $I(\Delta)$ is the Fourier transform of the intensity of the light source (globar) as function of wavenumber $I(\sigma)$, hence the name FTS. The source intensity $I(\sigma)$ implies that the beam follows a distribution related to its spectral radiance. Moreover, the light at different wavenumbers is incoherent and hence the intensity $I(\Delta)$ can be written as an integral over all wavenumbers of the light source (Liu, 2012) (Thorne, 1988):

$$\boldsymbol{I(\Delta) = \tfrac{1}{2}\int_0^\infty I(\sigma)[1+\cos(2\pi\sigma\Delta)]d\sigma}\,. \tag{22}$$

As can be seen from this equation, there are two parts present namely the unmodulated (DC) part and the modulated (AC) part i.e. the interferogram. The DC part is simply $\frac{1}{2} I_0$ and the AC part is given as follows (Liu, 2012) (Thorne, 1988):

$$\boldsymbol{I(\Delta) = \tfrac{1}{2}\int_0^\infty I(\sigma)\cos(2\pi\sigma\Delta)d\sigma}\,. \tag{23}$$

Now, in order to make the distribution $I(\sigma)$ as an even function, it can be shifted by $-\sigma_0$ to become symmetrical around a central wavenumber σ_0. In this manner, the interferogram could be written in terms of an exponential containing a real and an imaginary component (Liu, 2012) (Thorne, 1988):

$$\boldsymbol{I(\Delta) = \tfrac{1}{2}\int_{-\infty}^{\infty} I(\sigma)e^{i\pi\sigma\Delta}d\sigma}\,. \tag{24}$$

The resulting intensity $I(\Delta)$ will be a real function, as the imaginary odd part will disappear after integration and $I(\sigma)$ is a real even function. Evidently, one can see that the above equation implies a Fourier transform with $\alpha_{FT} = \frac{1}{2}$. However, the main point of interest is to acquire the intensity as function of wavenumber $I(\sigma)$. This can be recovered from the interferogram by taking the inverse Fourier transform (Liu, 2012) (Thorne, 1988):

$$\boldsymbol{I(\sigma) = 2\int_{-\infty}^{\infty} I(\Delta)e^{-i\pi\sigma\Delta}d\Delta}\,. \tag{25}$$

The interferogram is what is directly observed from the bolometer, however there will be a maximum retardation L as an infinite amount is not physical. Hence, the integration limits will change (Liu, 2012) (Thorne, 1988):

$$\boldsymbol{I(\sigma)' = 2\int_{-L}^{L} I(\Delta)e^{-i\pi\sigma\Delta}d\Delta}\,. \tag{26}$$

In addition, there will be a unit rectangular window function $\Pi\left(\frac{\Delta}{2L}\right)$ i.e. the detector function. Taking the Fourier transform of this window function yields the following (Liu, 2012) (Thorne, 1988):

$$\boldsymbol{F}\left[\Pi\left(\frac{\Delta}{2L}\right)\right] = \boldsymbol{2Lsinc(2L\sigma)}\,. \tag{27}$$

Consequently, the Fourier transform in equation 26 can be written in terms of a convolution of the detector function (Liu, 2012) (Thorne, 1988):

$$\boldsymbol{I(\sigma)'} = \boldsymbol{2Lsinc(2L\sigma)} * \boldsymbol{I(\sigma)}\,. \tag{28}$$

Here, $*$ denotes the convolution operator (Graham, 2009). In equations 27 and 28 respectively, the spectral resolution is limited by the full range of the movable mirror and hence the detector function has its first zero at (Liu, 2012) (Thorne, 1988):

$$\boldsymbol{\delta\sigma} = \frac{\boldsymbol{1}}{\boldsymbol{2L}}\,. \tag{29}$$

This quantity defines the spectral resolution of the interferometer and can therefore be easily controlled by modifying the range of the movable mirror.

4.2 Blue LED

4.2.1 Interferograms

The basic setup for installation of the Blue LED includes a small optical rail with two lenses and the silicon slab together with an absorber containing an aperture of $10\ mm$. The two lenses include a hyperbolic lens as well as a spherical lens. The hyperbolic lens was used to collimate the light and the spherical lens was used to focus the light onto the aperture. See figure 14 for the overview of the experimental setup together with the optical scheme in figure 15.

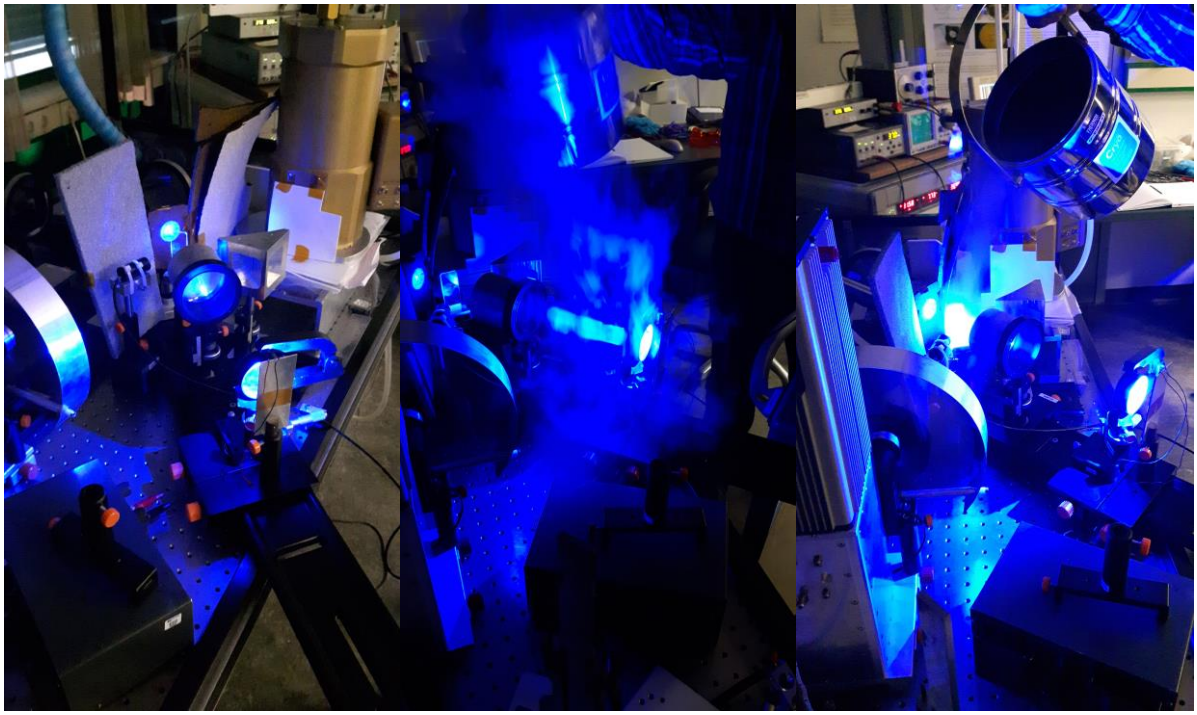

Figure 14: Experimental setup for optical illumination of a silicon slab with a blue LED as part of the FTS setup.

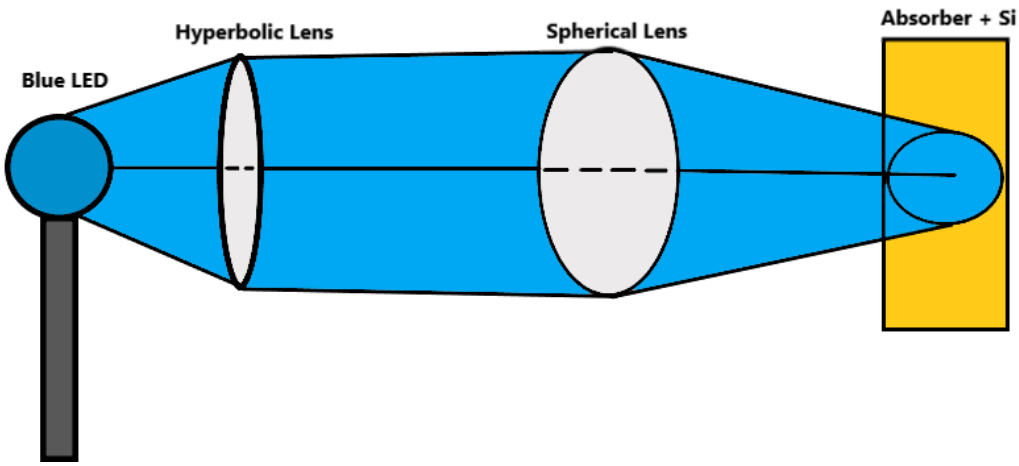

Figure 15: Schematic overview of the optics as integrated into the FTS setup.

By means of the FTS setup, several interferograms could be measured using different intensities of light. This was controlled by managing the input current for the LED. In fact, two blue LED's were stitched together in series to increase the intensity. The input current I_{in} was varied from 0 to $1A$ in steps of $0.2A$. Table 2 includes an overview of the most important settings that were required to carry out the experiment before any measurements were performed.

Lock-in voltage (Si/Unill.)	Globar voltage/current	Range	Step size [5 μm]	Dwell time	Integration time
42.1 mV	*3.74*V/*5.99*A	*10.000* steps	*20*	*0.4*s	*0.1*s

Table 2: Parameter settings for the FTS experiment with a blue LED.

Taking into account these parameters, in total eight interferograms were measured including three separate dark measurements. The dark measurements were carried out after the measurements with $I_{in} = 1A$ (OFF), $I_{in} = 0.6A$ (OFF1) and $I_{in} = 0.2A$ (OFF2). In figure 16 the main results are depicted including the light measurements together with the first dark measurement (OFF).

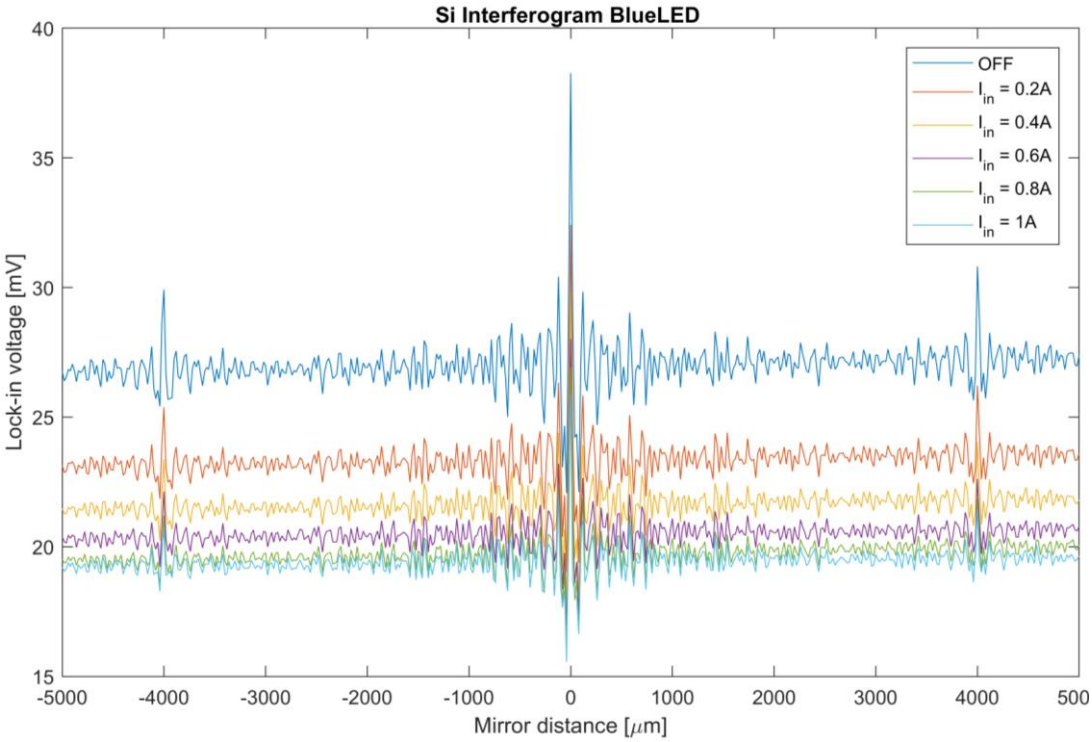

Figure 16: Interferograms of the silicon light measurements using discrete steps of input current for the blue LED. The first dark measurement has been incorporated as a reference.

Characteristically, one observes the central peak in the middle which corresponds to the central wavenumber σ_0 of the THz beam i.e. the point of highest constructive interference. In addition, one observes that the interference pattern is nicely symmetric. Interestingly, there are some symmetric

small peaks present which corresponds to standing waves of the THz beam that are produced in the Si slab. One of the significant points of interest is whether these peaks shift when illuminating the Si slab. This would correspond to a change in relative permittivity ε_r and hence changes the complex refractive index $\tilde{n}$ as the Si slab becomes conductive. According to the measured interferograms as depicted in figure 16, this does not turn out to be the case. One of the motives for this could be related to the penetration depth of blue light. Since the penetration depth of blue light is limited, a region of electron plasma will only form close to the surface of the Si slab. This would imply that a small fraction of the Si slab becomes conductive whereas the rest of the Si slab still remains high resisistivy. A change in ε_r over such a small region would not be visible in the interferograms, possibly only with very high resolution measurements.

Lastly, the results of the dark measurements are illustrated together in figure 17 i.e. OFF, OFF1 and OFF2. This confirms that all three separate dark measurements coincide and that no external influences have changed the settings during the experiment.

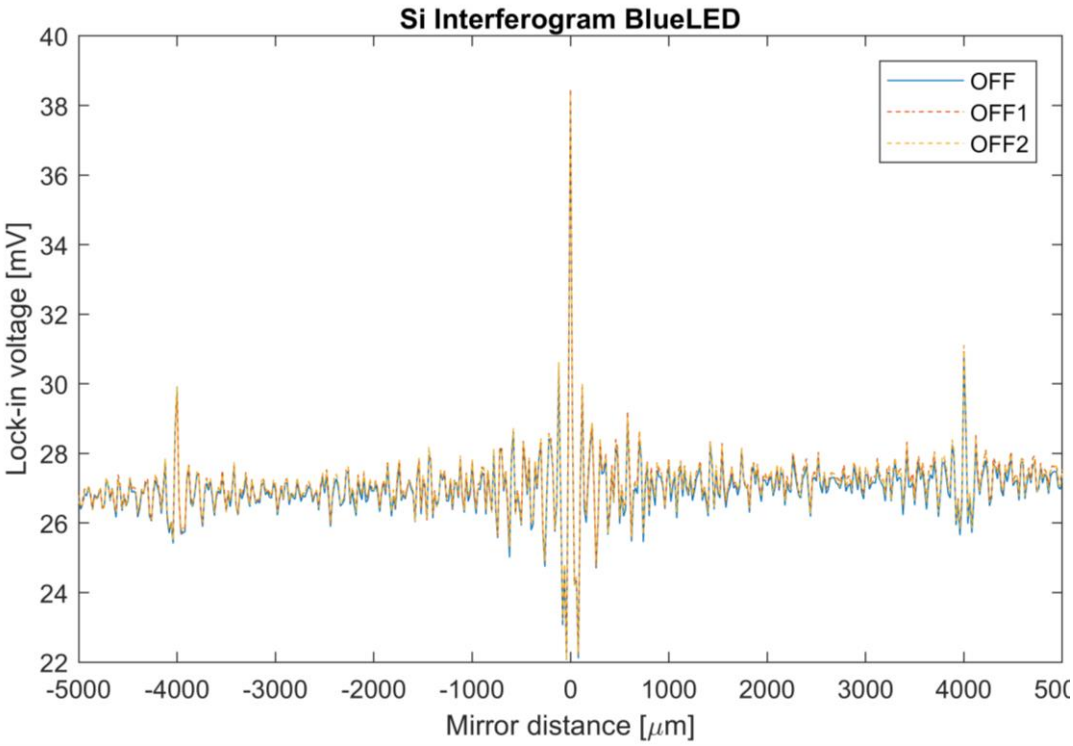

Figure 17: Interferograms of the three dark measurements performed in the blue LED experiment.

4.2.2 FT Interferograms

Based upon the interferograms of section 4.2.1, the (discrete) Fourier transform has been taken in order to look at the frequency dependence of the intensity from the globar. Taking into account the amount of steps ($10.000\ steps$) as well as the step size ($5\ \mu m$), the spectral resolution becomes:

$$\delta\sigma = \frac{1}{(2\times 0.05)*10^2} = 0.1\ cm^{-1}.$$

$$\delta f = 3\ GHz\ .$$

In figure 18, the FT interferograms are shown for the first dark measurement (OFF) together with the blue LED illumination in discrete steps of the input current I_{in}.

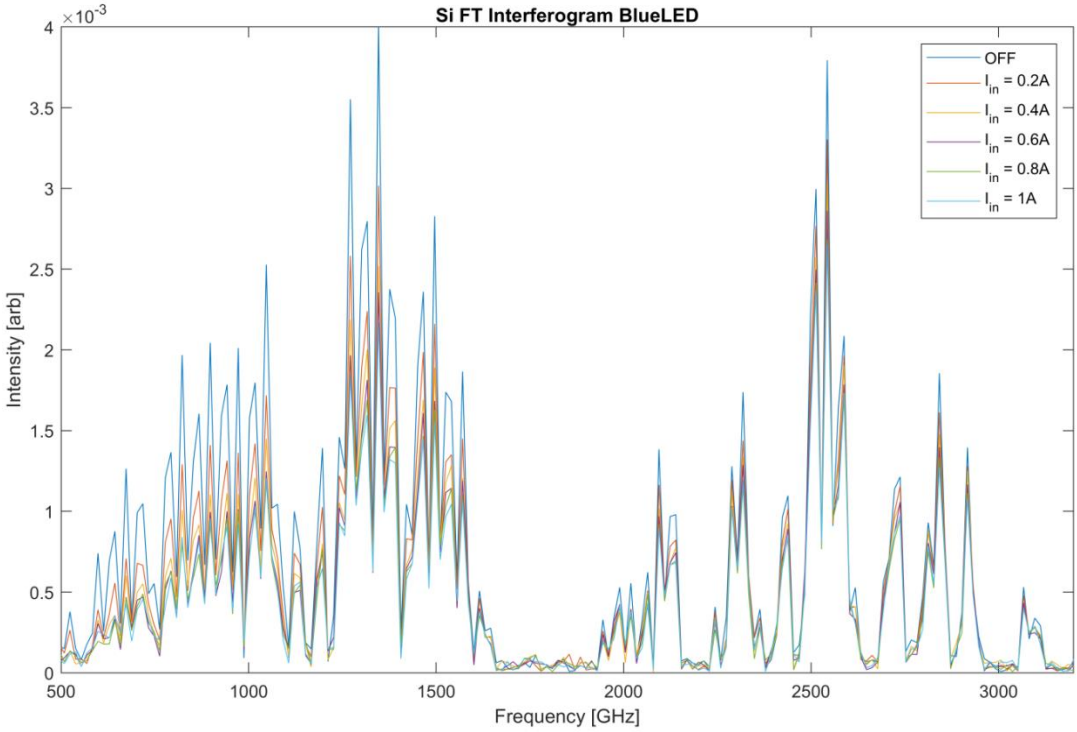

Figure 18: Fourier transform interferograms of the blue LED experiment showing the globar intensity's frequency dependence.

Several peaks are visible at specific frequencies corresponding to material properties of the Si slab. In particular, around $1.1, 1.3$ and $2.6\ THz$ the intensity rises sharply. These features could be characteristic to the type of illumination and hence it would be interesting to compare the results with the other light sources. Seemingly, there is no frequency shift present, although the peaks are decreased in magnitude. Perhaps there could be a scaling involved (i.e. a change in Q-factor), however this would only be visible with another measurement setup such as a high-resonance cavity (Dickmann, 2003).

Subsequently, the FT interferograms of the dark measurements have been plotted together. See figure 19 for the graph of the measurements.

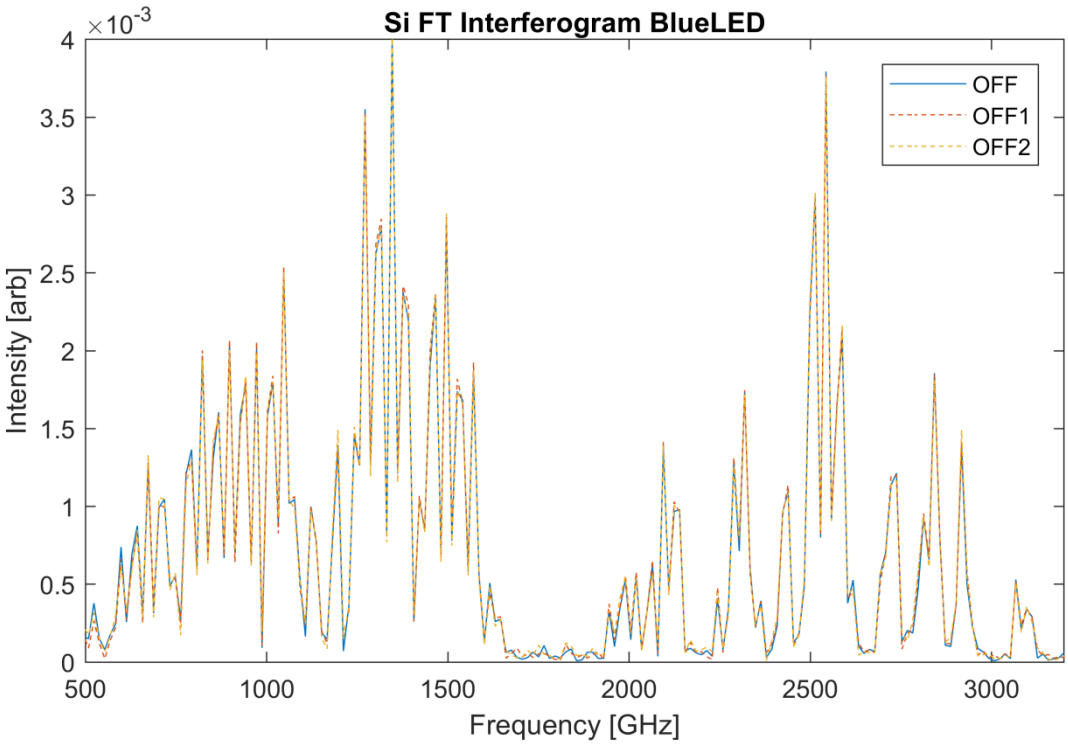

Figure 19: FT interferograms of the three dark measurements in case of the blue LED experiment.

As can be observed, the curves lie closely together as was also the case in the spatial domain. There are only minor differences present at some peaks compared to the first dark measurement (OFF). This result confirms that there is no significant environmental- or thermal effect present that alters the properties of the Si slab besides the optical illumination of the blue LED.

4.2.3 Intensity Ratios

On the basis of the intensity vs frequency plots, also a ratio can be taken with respect to the dark measurements that have been carried out. In this case, one would acquire the intensity ratio vs frequency plots, which specifies the frequency dependence of the THz beam more accurately. Particularly, a low intensity ratio corresponds to a higher transmittance of the THz beam. The intensity ratios vs frequency for the input current of $I_{in} = 1A$ is shown in figure 20. Note that the intensity ratio is expressed in decibels $[dB]$ relative to the dark measurements. Moreover, a more specific range has been chosen as this range is of most interest for future measurements related to the ALMA project. As can be seen from the graphs, the attenuation is in the order of -5 to -6 dB which is relatively low. This would be just sufficient to carry out the noise temperature measurements. There seems to be a slight increasing trend with frequency as well which could be intrinsic to features of the light source. So at lower frequencies, the attenuation is slightly larger as compared to higher frequencies. This might actually be favourable as the local oscillator used for future measurements is operated around $600 - 750\ GHz$.

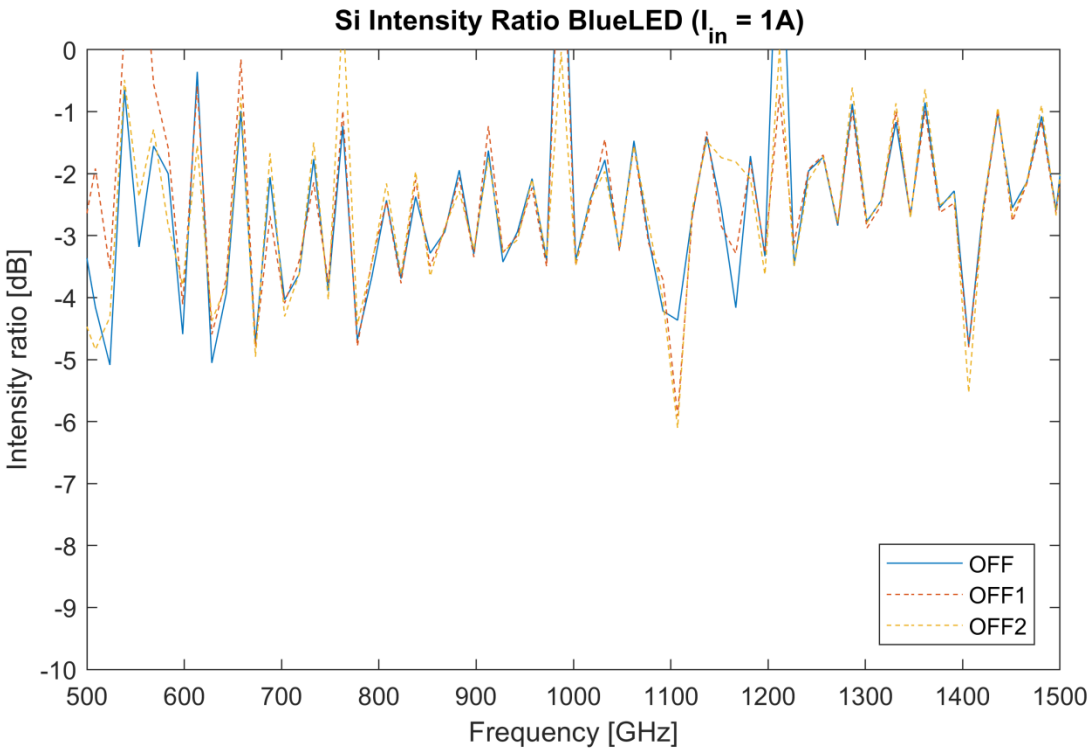

Figure 20: Intensity ratio plots relative to the three dark measurements for the highest illuminance of the blue LED ($I_{in} = 1A$).

4.3 Microscope Light

4.3.1 Interferograms

Subsequent to the measurements with the blue LED, a different light source has been used namely the microscope light which includes a white light source connected to an optical fibre. Similar to the photodiode calibration measurement, the light was moved backwards from the Si slab in discrete steps and at each step an interferogram has been taken. See figure 21 for the results. These measurements were carried out in the same experiment and hence the parameters as stated in table 2 are still applicable. However, one noticeable effect that occurred was that the Lock-in voltage steadily dropped over time without performing any measurements. There could be various explanations for this occurrence, although the exact nature remains unknown. Nonetheless, this effect has been taken into account and does not affect the results of the interferograms in any significant way.

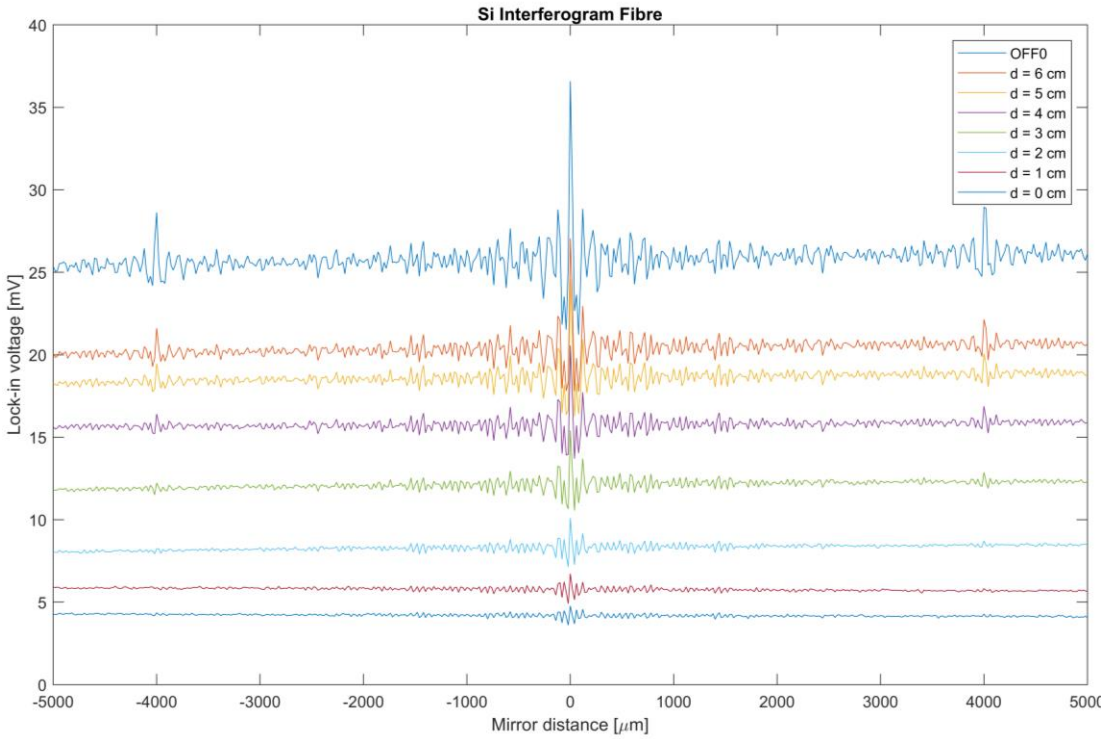

Figure 21: Interferograms of the light measurements in case of the microscope light (halogen lamp with optical fibre). OFF0 corresponds to the dark measurement after the light measurement of $d = 0\ cm$ was carried out (closest position possible without obscuring the THz beam).

From figure 21, it can clearly be observed that the THz beam is supressed significantly. Not only has the Lock-in voltage dropped down, also the central peaks as well as the smaller Si peaks have been decreased in magnitude. At $d = 0\ cm$, the predominant part of the signal has been completely suppressed. This amount of suppression would be sufficient enough to allow the experiment of the noise temperature to be conducted. Similarly, no change in either the central or the Si peaks have been observed during the measurements. Hence, a different high resolution experiment might be required to observe this effect involving a high resonance cavity. In this way the (change in) Q-factor can be determined very accurately.

In the same way as during the blue LED measurements, also here three different dark measurements have been done namely after $d = 0\ cm$ (OFF0), $d = 3\ cm$ (OFF1) and $d = 6\ cm$ (OFF2). The results can be found in figure 22. As opposed to the measurements in the blue LED experiment, here the three dark measurements do differ from each other. An explanation for this could be related to the amount of infrared light coming from the optical fibre. The infrared light might alter the temperature of the Si slab and hence changes the material properties. This change could lead to more absorption of the THz beam, so this phenomenon could be a pure temperature effect. One way to justify this statement is that the signal for the dark measurements increases while the light is moved away from the silicon slab. This would imply that less infrared light enters the Si slab, the temperature would be decreased and hence the Lock-in voltage would increase. This is precisely the case as can be observed in figure 22.

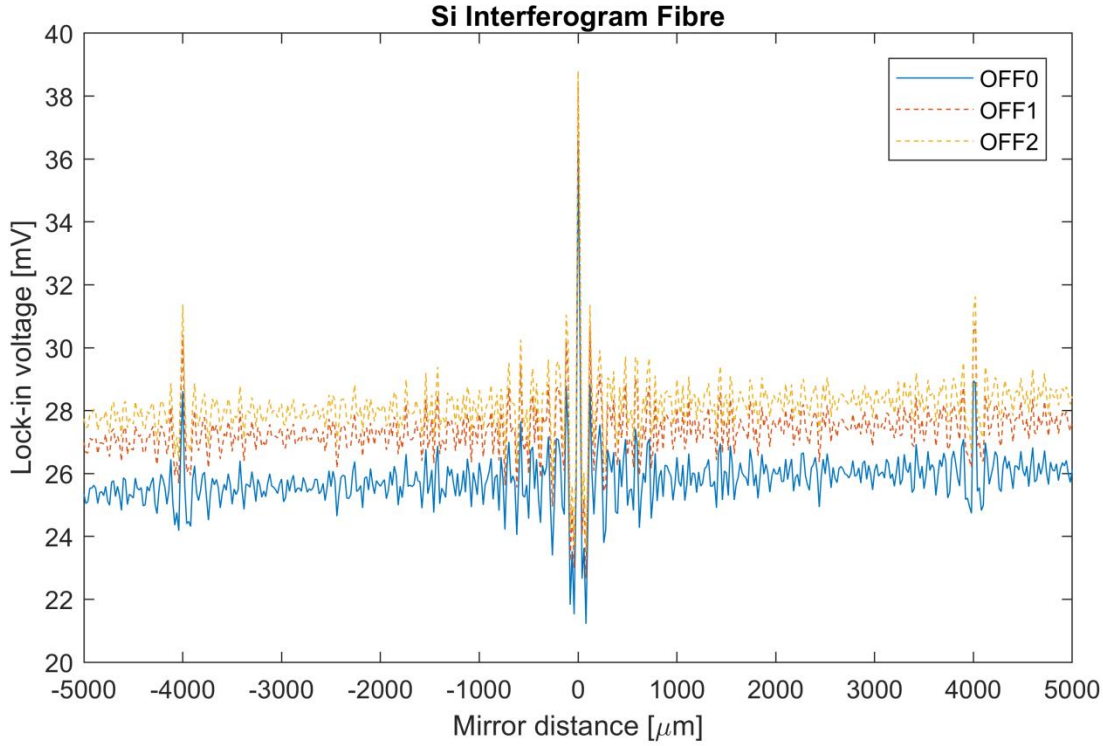

Figure 22: Interferograms of the three dark measurements performed with the microscope light (halogen lamp with optical fibre).

4.3.2 FT Interferograms

Also for the interferograms as illustrated in section 4.3.1, a Fourier transform has been taken. Since the amount of steps is the same as was the case for the blue LED, the spectral resolution is similar as well. In figure 23, the FT interferograms are depicted for several illuminations of the microscope light acquired by moving the optical fibre backwards from the Si slab.

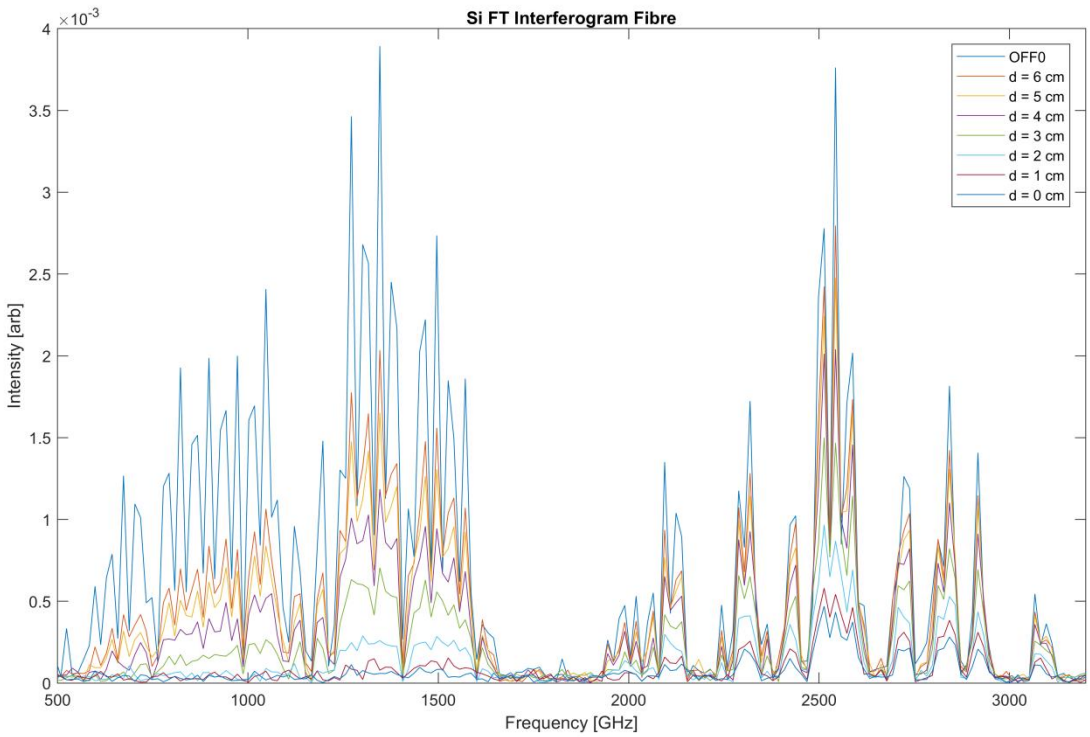

Figure 23: FT interferograms of optical illumination of a Si slab in the FTS using a microscope light (halogen lamp with optical fibre).

In comparison to illumination with the blue LED, the curves lie more apart from each other. This implies that the amount of attenuation from the microscope light is significantly higher. Moreover, the infrared light as well as the UV light is filtered out due to the optical fibre. Hence, the difference can be partly attributed to heating of the Si slab by the high optical power of the microscope light.

Subsequently, the FT interferograms of the three different dark measurements were constructed. See figure 24 for the results. Noticeably, the trends of the curves are similar to each other although the amplitudes of the peaks are different. The peaks of the 2nd and 3rd dark measurements are slightly higher as compared to the 1st dark measurement. Hence, the amplitude difference that was present in the spatial domain is translated into the frequency domain accordingly. As discussed before, this could be due to a heating effect of the Si slab.

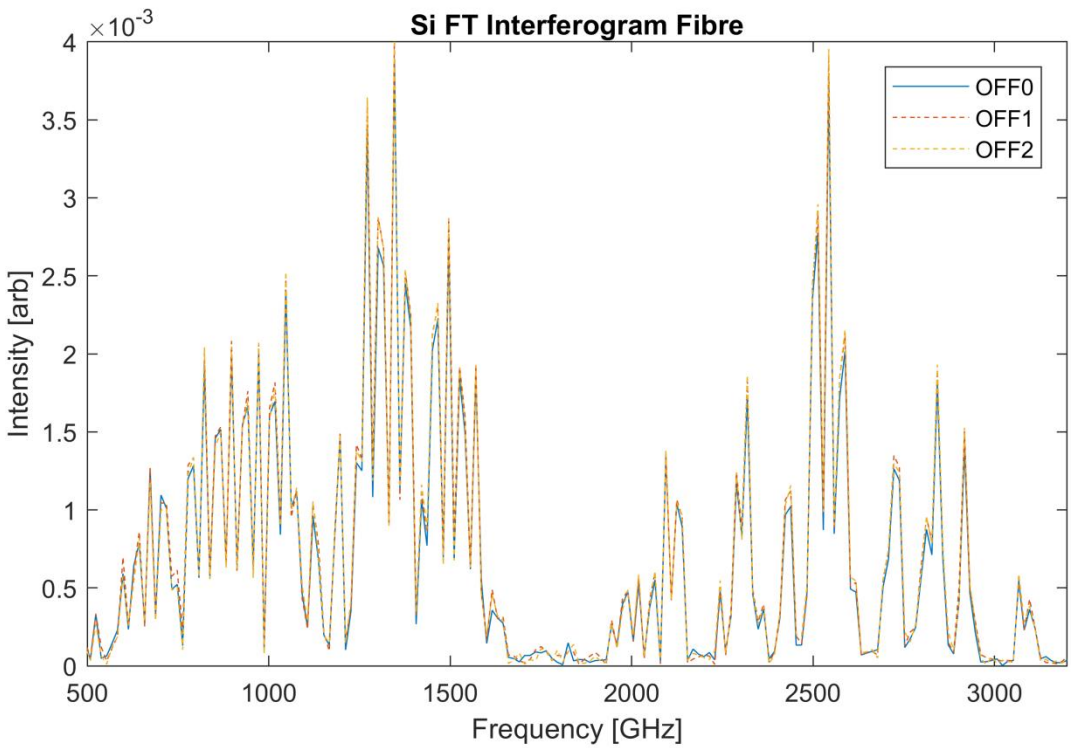

Figure 24: FT interferograms of the three dark measurements as part of the microscope light (halogen lamp with optical fibre) experiment at $d = 0\ cm$ (OFF0), $d = 3\ cm$ (OFF1) and $d = 6\ cm$ (OFF2).

4.3.3 Intensity Ratios

In case of the microscope light, two intensity ratios have been computed relative to the dark measurement at $d = 0$ (OFF0), namely $I(d = 0\ cm)/OFF0$ and $I(d = 3\ cm)/OFF0$. The latter intensity ratio has been included in order to make a proper comparison with the blue LED experiment. Hence, the amount of attenuation is similar to the blue LED with $I_{in} = 1A$. See figure 25 for an overview of the results. The attenuation for the intensity ratio at $d = 0$ is significantly higher as was the case for the blue LED, with values in the order of -15 dB. Interestingly, there seems to be a sharp peak around $1200\ GHz$, which is most likely due to absorption from H_20 in the environment. In this case there does not seem to be a trend that the amount of attenuation is

increased at lower frequencies. Rather, the trend of the curve goes down up until around $1\ THz$ and then goes slightly up in magnitude.

Interestingly, the curve at $d = 3\ cm$ is rather different from the curve at $d = 0\ cm$ and seems to follow the trend as was the case for the blue LED experiment i.e. the transmission appears to increase at higher frequencies. In addition, the difference in magnitude of the intensity ratio between the two curves appears to become larger at higher frequencies, whereas at around $650\ GHz$ the curves coincide. Consequently, these findings require a more rigorous study to describe the underlying physical principles.

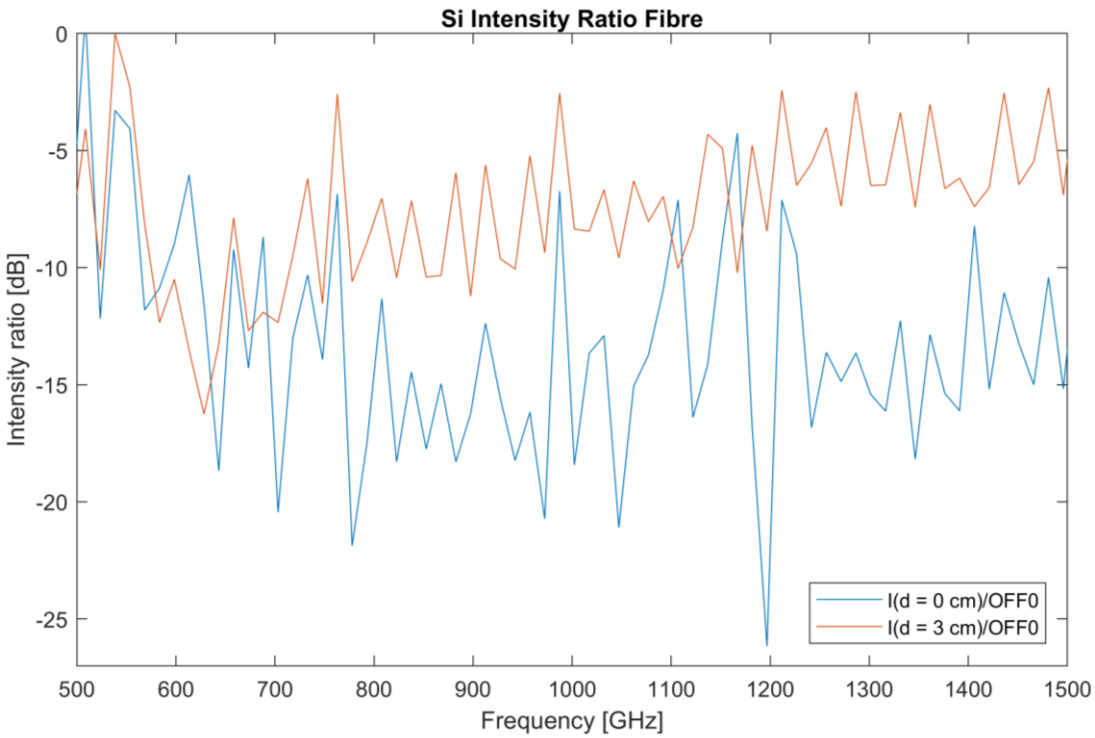

Figure 25: Intensity ratio versus frequency for $d = 0\ cm$ and $d = 3\ cm$ of the microscope light (halogen lamp with optical fibre) relative to the dark measurement at $d = 0\ cm$ (OFF0).

4.4 Halogen Lamp

4.4.1 Interferograms

In this experiment, a halogen lamp including an internal reflector has been used as a light source for illumination of the Si slab. In the same way as the microscope light, the halogen lamp is moved out of focus from the Si slab in discrete steps. Steps of $5\ cm$ were taken from 0 to $20\ cm$, where $0\ cm$ was the optimally tuned position. In figure 26 an overview of the setup is illustrated together with the corresponding optical scheme in figure 27. The aperture in the absorber material is $10\ mm$ as well. Moreover, an optical beam splitter (microscope glass) has been installed to do a simultaneous calibration measurement with the photodiode. The microscope glass has a reflectance of approximately 10%. Since this experiment was done separately from the previous measurements, the parameter settings were changed. The most significant parameter settings of this experiment are listed in table 3.

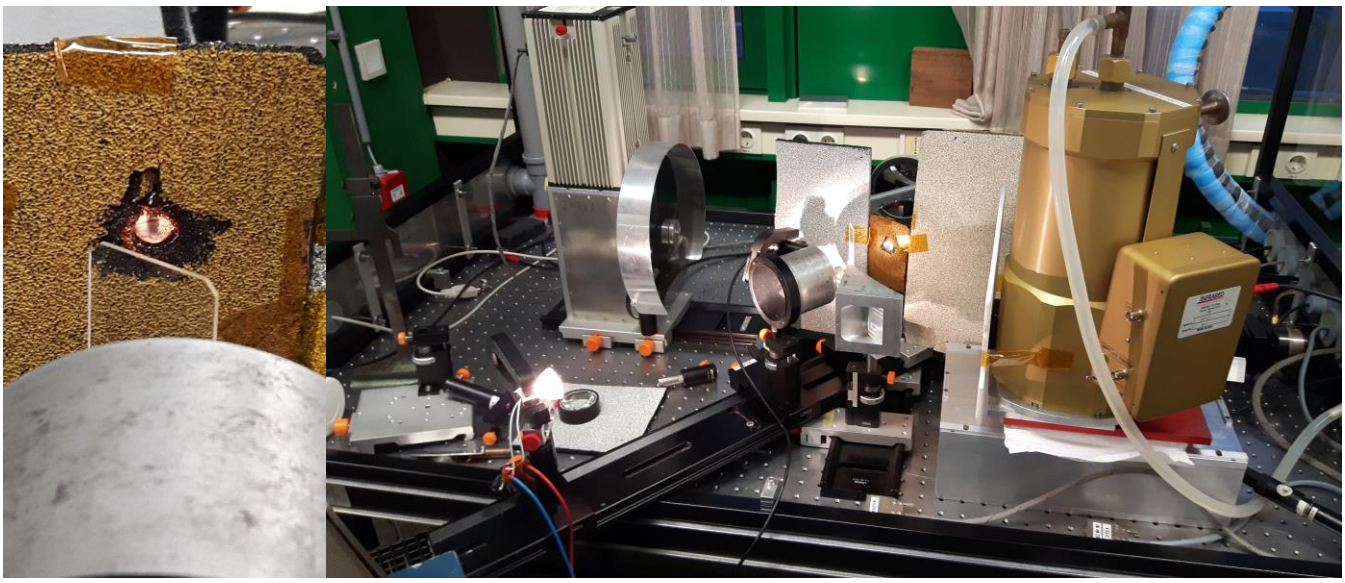

Figure 26: Experimental setup for optical illumination of a silicon slab with a halogen lamp as part of the FTS. Note that an optical beam splitter was installed for calibration purposes.

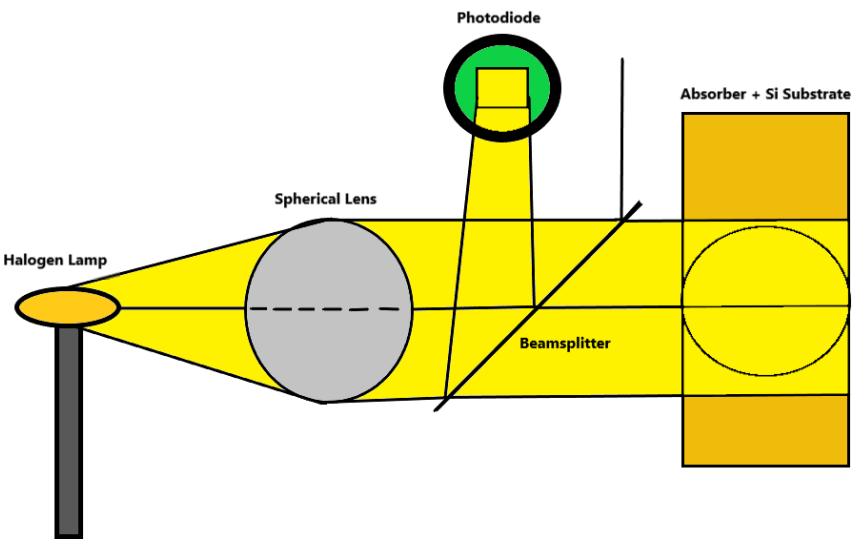

Figure 27: Optical scheme for the halogen lamp in the FTS setup.

Lock-in voltage (Si/Unill.)	Globar voltage/current	Range	Step size [5 μm]	Dwell time	Integration time
9.5 mV	*3.73V/5.99A*	*40.000* steps *10.000* steps	*20*	*0.4*s	*0.1*s

Table 3: Parameter settings for the FTS experiment with a halogen lamp.

Two different ranges have been used for measuring the interferograms namely a high resolution scan including 40.000 steps and a normal resolution scan including 10.000 steps. At each interval of $5\ cm$, both a light and a dark measurement have been performed. In addition, a Gore-Tex low-pass filter with a cut-off around $3\ THz$ has been applied to the input of the bolometer filtering out undesirable environmental infrared radiation. Hence, the Lock-in voltage is less as compared to previous measurements done with the blue LED and the microscope light. The high resolution interferogram can be found in figure 28 together with the dark measurement carried out at the optimally tuned position ($d\ =\ 0\ cm$).

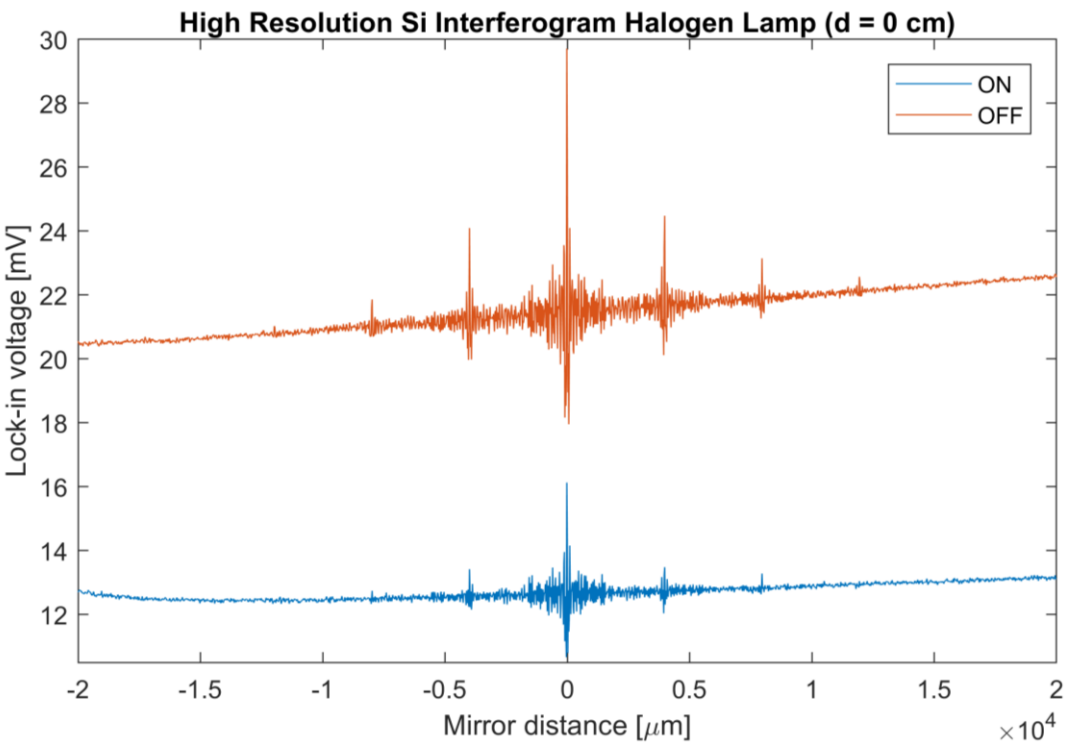

Figure 28: High resolution (40.000 steps) interferogram for optical illumination of a Si slab with a halogen lamp. The central peak as well as several Si peaks can clearly be observed.

Interestingly, more silicon peaks can be observed than before corresponding to the standing waves. However, when applying a scale factor to the light measurement (ON), the peaks do not seem to be shifted either. Hence, using the FTS setup a change in relative permittivity ε_r is not feasible when using the current settings. Subsequently, the light-dark measurements at different intervals were carried out with normal resolution. The interferograms of these measurements are depicted in figure 29.

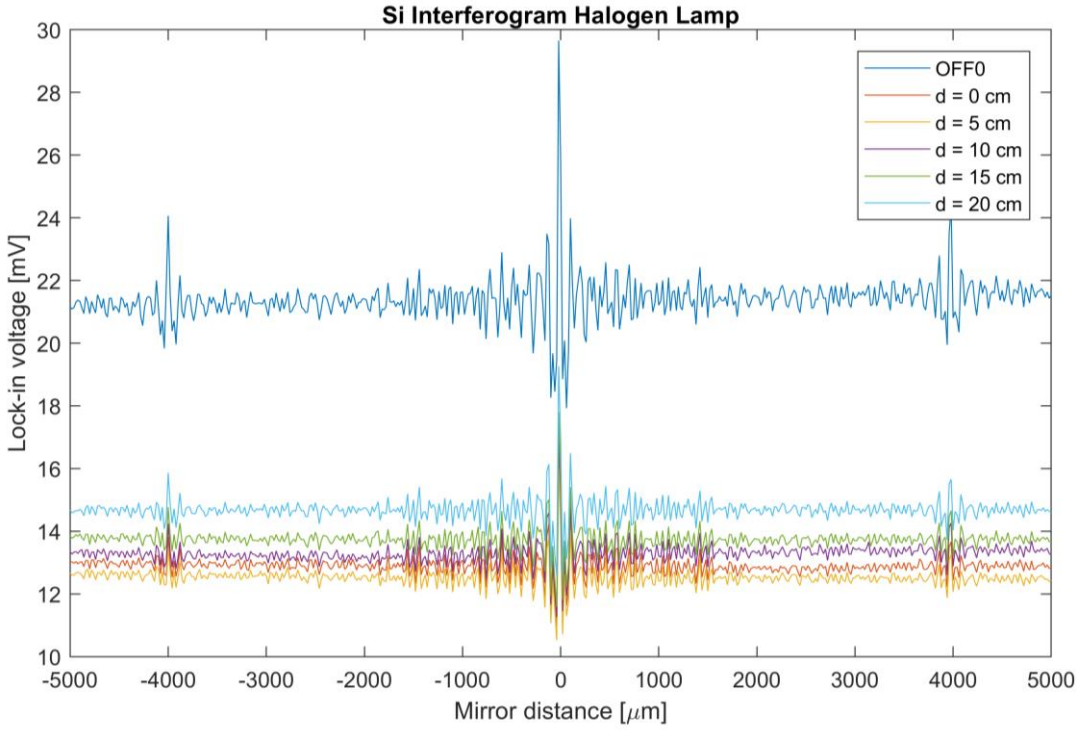

Figure 29: Normal resolution (10.000 steps) interferograms with optical illumination of a Si slab using a halogen lamp. The halogen lamp was moved out of focus in $5\ cm$ steps up to $20\ cm$.

Noticeably, the $d = 0\ cm$ point does not correspond to the optimally tuned position. Instead, the position at $d = 5\ cm$ seems to yield a slightly larger attenuation. In these interferograms only two Si peaks are visible as the smaller peaks are out of range. The attenuation appears to be lower as compared to the microscope light measurements, although higher as compared to the blue LED measurements. Nonetheless, the attenuation is still large enough to carry out the noise temperature measurements so a proper comparison can be made. Subsequently, all dark measurements have been plotted together in one graph, which are illustrated in figure 30.

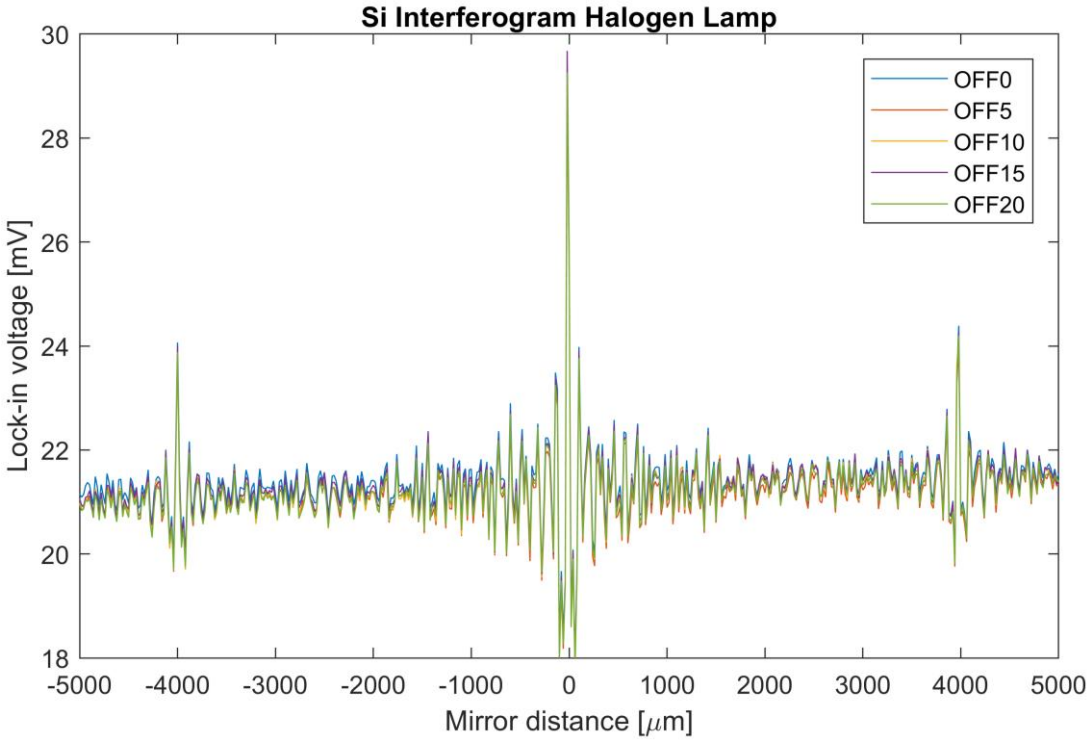

Figure 30: Interferograms of the dark measurements performed at each distance interval using a halogen lamp.

The results coincide fairly well although there is a slight difference in magnitude among the measurements. Once more, this could be a temperature effect as well due to the infrared radiation from the halogen lamp. The difference as compared to the microscope light might be that less infrared arrives at the Si slab, as with the halogen lamp a lens was used to focus the light. In case of the microscope light the optical fibre was only moved out of focus without further optics. So far, three different light sources have been used for the measurements. In the next section, the Fourier transform of the interferograms for these measurements will be discussed in more detail.

4.4.2 FT Interferograms

In this section, the FT interferograms of the measurements with the halogen lamp will be discussed. Here the spectral resolution is also the same ($3\ GHz$) which leads to a more convenient evaluation among the experimental results. See figure 31 for the results.

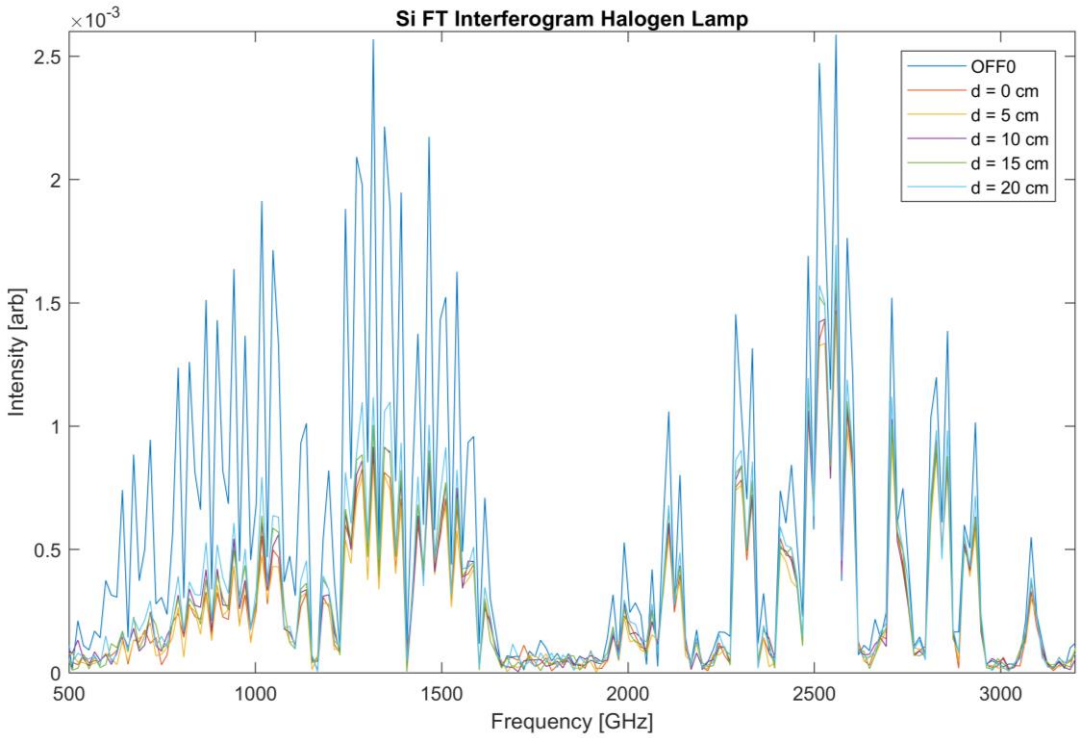

Figure 31: FT interferograms for illumination of a Si slab with a halogen lamp using the FTS setup.

As can be seen from the graph, the intensity is lower as compared to the previous measurements as an additional Gore-Tex (IR) filter was applied apart from the internal filter inside the bolometer. Therefore, the Lock-in voltage dropped and hence the intensity as well. Nevertheless, there is a fair amount of attenuation present, which would suffice for the noise temperature measurements. In addition, there seems to be little variance present among the curves at varying distances. Perhaps taking steps of $10\ cm$ was a better choice, although this justifies that the reflector inside the halogen lamp bundles the light rather efficiently.

Subsequently, the high resolution FT interferogram ($40.000\ steps$) has been measured as well. This has been illustrated in figure 32.

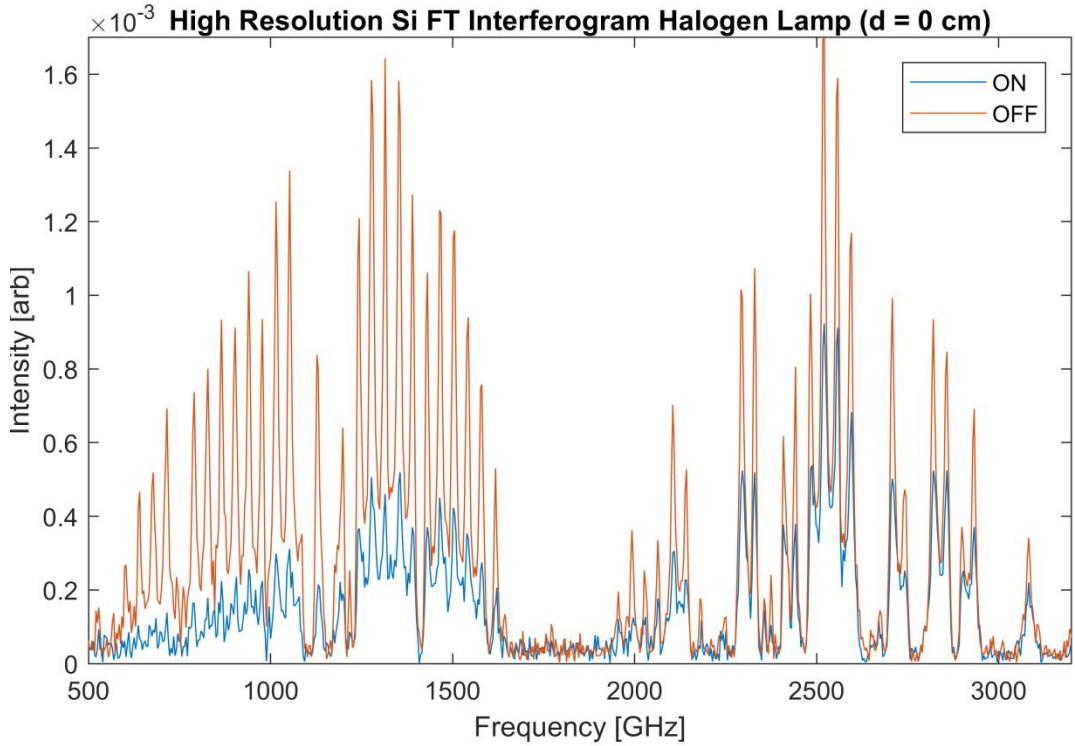

Figure 32: High resolution FT interferogram of Si slab illumination using a halogen lamp including an internal reflector. Both the light and dark measurements are shown at the optimally tuned position ($d = 0\ cm$).

In this case the corresponding resolution becomes as follows:

$$\delta\sigma = \frac{1}{(2\times0.2)\times10^2} = 0.025\ cm^{-1}\ .$$

$$\delta f = 0.75\ GHz\ .$$

Hence, more Si features are present which could be useful for future detailed analysis. Finally, the FT interferograms of the dark measurements are plotted together which can be found in figure 33. The curves seem to coincide rather well, with some minor differences in amplitude present. In all likelihood, the halogen lamp produces less IR radiation as compared to the microscope light and consequently the heating effect is less apparent in this case.

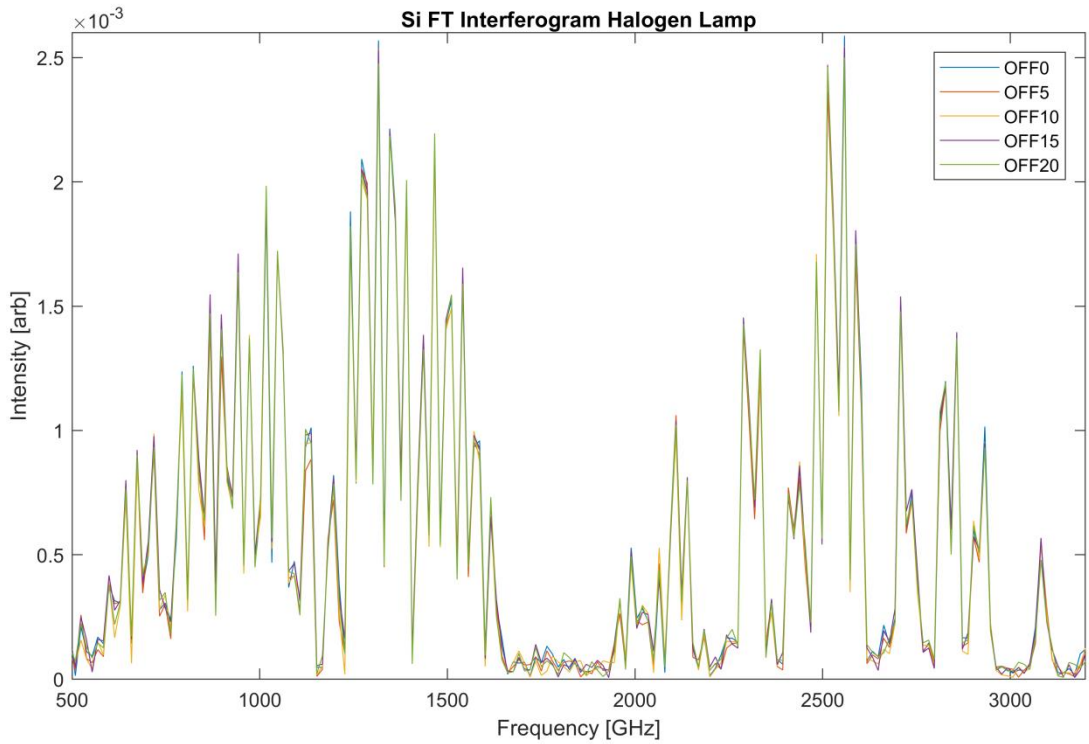

Figure 33: FT interferograms of all dark measurements involved in the Halogen lamp experiment.

4.4.3 Intensity Ratios

Lastly, the intensity ratios for the halogen lamp have been computed relative to the dark measurements done at each distance interval. For the highest illuminance, both a high- and normal resolution measurement has been carried out. The results can be found in figure 34.

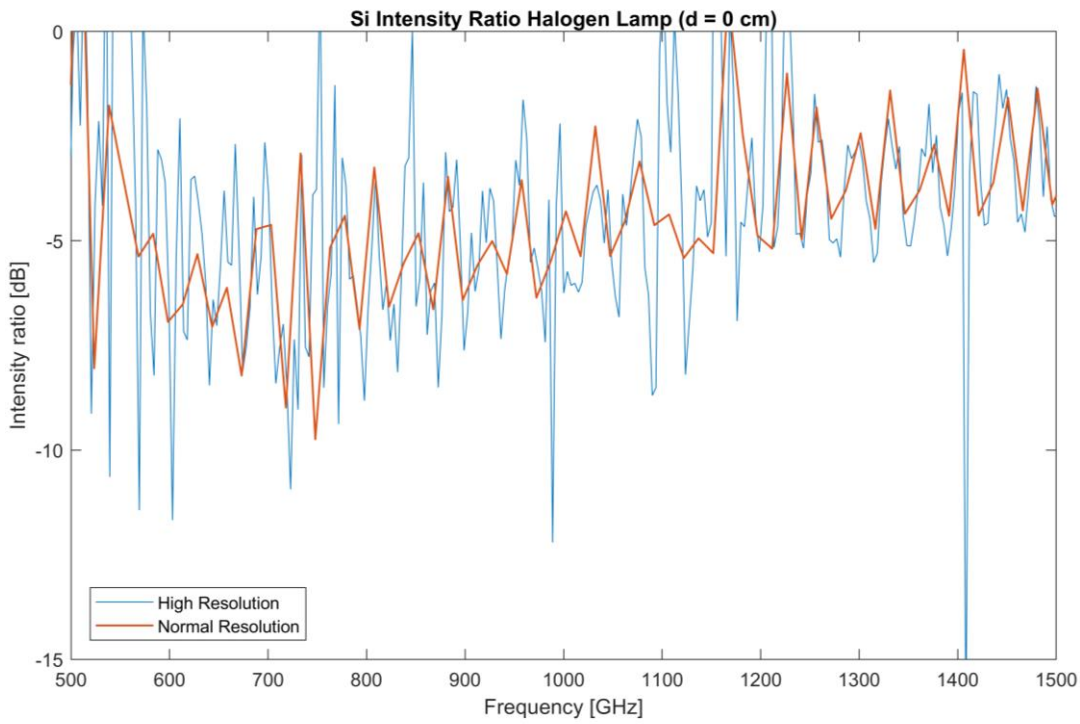

Figure 34: High resolution ($40.000\ steps$) vs normal resolution ($10.000\ steps$) intensity ratios measured for the highest illuminance of the halogen lamp ($d\ =\ 0\ cm$).

Remarkably, there are many more steep peaks present in case of the high resolution measurement. The amplitudes are significantly higher as compared to the normal resolution measurement. From this graph it certainly can be observed that the attenuation at lower frequencies is the highest, which holds true for both curves. Hence, the features that are present in this graph can be studied for a more detailed analysis of the Si properties.

5. Heterodyne Receiver Experiment

5.1 Experimental Setup & Settings

In this experiment, the goal is to examine whether optical illumination of a Si substrate contributes to the overall noise temperature in a heterodyne receiver setup. The optical illumination of the Si substrate is used to spatially modulate the THz radiation from the Local Oscillator (LO). In this manner the intensity of radiation can be regulated accurately. Moreover, more sophisticated applications could be realised such as THz beam steering in conjunction with a phased array feed. A schematic overview of the experimental setup has been illustrated in figure 35.

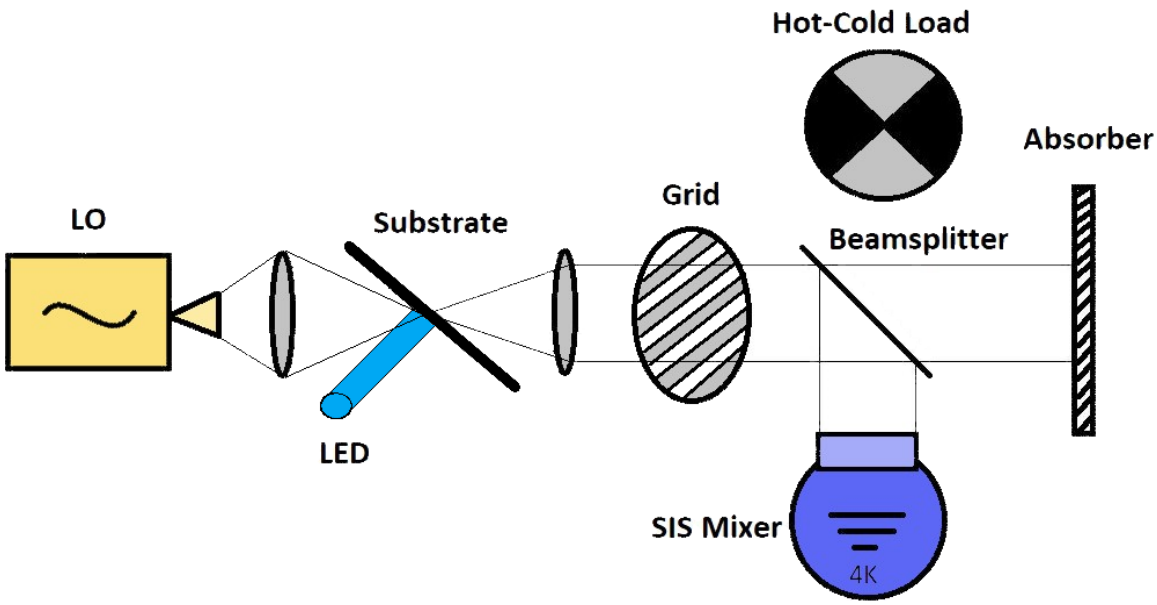

Figure 35: Overview of the setup as used in the heterodyne receiver experiment using optical illumination of a Si substrate.

The LO in this setup is regulated by a Rhode & Schwarz Surface Mounted Package (R&S SMP) frequency generator using two frequency multipliers. Each multiplier has an amplification factor of twenty-seven and the RS SMP base frequency is set to $12\ GHz$. Hence, the operation frequency of the LO is given by: $12 \times 27 \times 2 = 648\ GHz$. First of all, the I-V curve of the Superconductor-Insulator-Superconductor (SIS) junction needs to be optimised without using the Si substrate and any LO power i.e. unpumped operation. The main challenge here is to remove the Josephson current which essentially is the quantum tunnelling of cooper pairs (i.e. paired states of electrons). This phenomenon is based upon the phase difference in the corresponding electron wave functions on both sides of the junction and can be counteracted by applying a magnetic field (MIT, 2003). In figure 36, three different I-V curves are illustrated. The first curve is the unpumped curve with suppressed Josephson current. The second curve is the (over)pumped curved with slightly less well suppressed Josephson current. Finally, the third curve is the optimally pumped curve which is around 30% of the (over) pumped curve. In this manner, the longevity of the LO is sustained. The power is controlled by rotating the grid as can be observed from the figure.

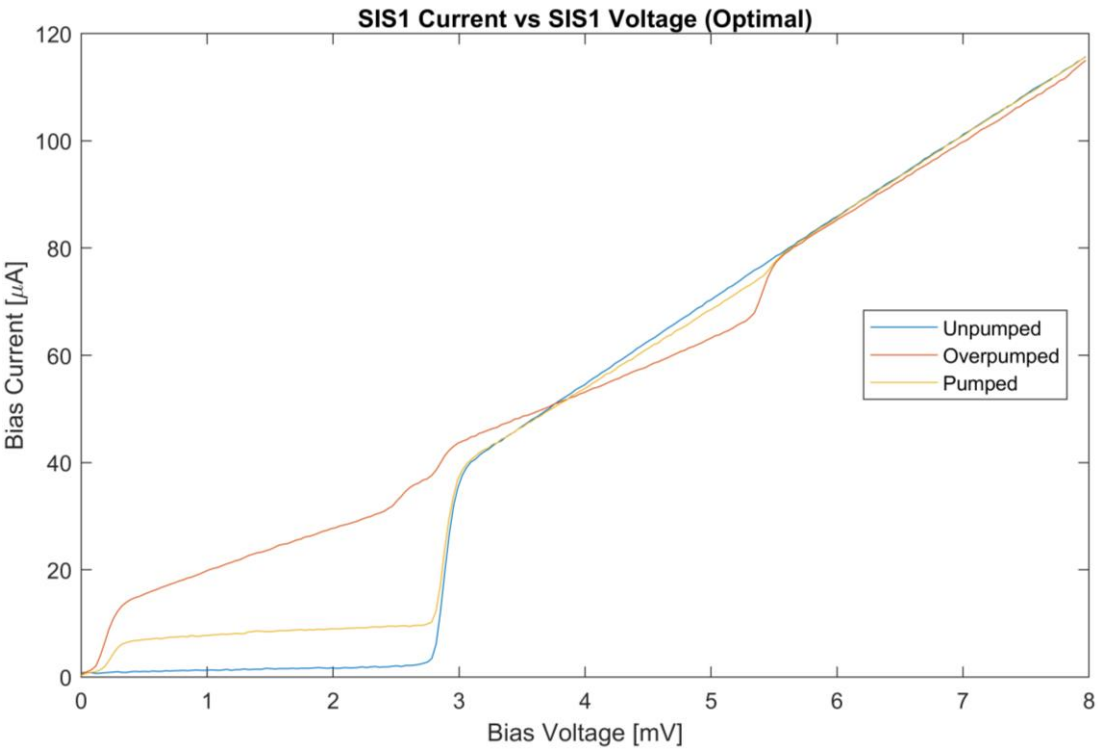

Figure 36: I-V curves of the SIS mixer depicting three different pumping levels. Note that the Josephson current has been suppressed.

Essentially, the step width of the I-V curve is dependent on the frequency of the LO. The current step relative to the unpumped curve is due to photo-assisted tunnelling of electrons. The LO actually creates higher (and slightly lower) energy states that are available to be occupied (breaking degeneracy) (Tucker, et al., 1985). According to theory, in order to produce a quasiparticle current the bias energy should be at least two times the energy gap i.e. (Baryshev, 2015):

$$\boldsymbol{eV_b \geq 2\Delta}\,. \tag{30}$$

Here, V_b is the bias voltage and Δ is the energy gap of the superconductor material (e.g. $NbTiN$). Note that this result holds true for the $0K$ temperature limit. Subsequently, the voltage can be specified relative to the energy gap in terms of integer-multiple current steps. Effectively, the width of the current step is determined by the photon energy hv, so that (Baryshev, 2015):

$$\boldsymbol{V} = \Delta - \frac{\boldsymbol{nhv}}{\boldsymbol{e}}. \tag{31}$$

Here, n is the number of current steps and e is the elementary charge. In this experiment, there is only one photo-assisted current step and hence $n = 1$.

Subsequently, the height of the I-V curve is dependent on the LO power. The LO power is proportional to the square of the photon energy and is also dependent on the slope of the I-V curve i.e. $R_N = dI/dV$. Hence, the LO power is given by (Baryshev, 2015):

$$\boldsymbol{P_{LO}} \sim \frac{(\boldsymbol{h\nu/e})^2}{\boldsymbol{R_N}}. \tag{32}$$

As soon as the I-V curve is optimised, the diaphragm with the Si substrate could be installed. Since the Si substrate brings about standing waves from the LO, the SIS current will vary as function of LO frequency generated by the RS SMP frequency generator. Therefore, the LO frequency needs to be optimised for a particular transmission peak at which the Si substrate is largely transparent for the corresponding frequency. This can be nicely seen in figure 37. In this case, the frequency is adjusted to the first transmission peak as it is slightly higher in magnitude compared to the second peak. Nevertheless, in general any transmission peak could be taken. Specifically, this implies that $f_{SMP} = 11.83\ GHz$ corresponding to a LO frequency of $f_{LO} \approx 639\ GHz$. Note that the absorber material with aperture of $d = 10\ mm$ was installed before the measurement was carried out and a fixed bias voltage has been used of $V_b = 2mV$.

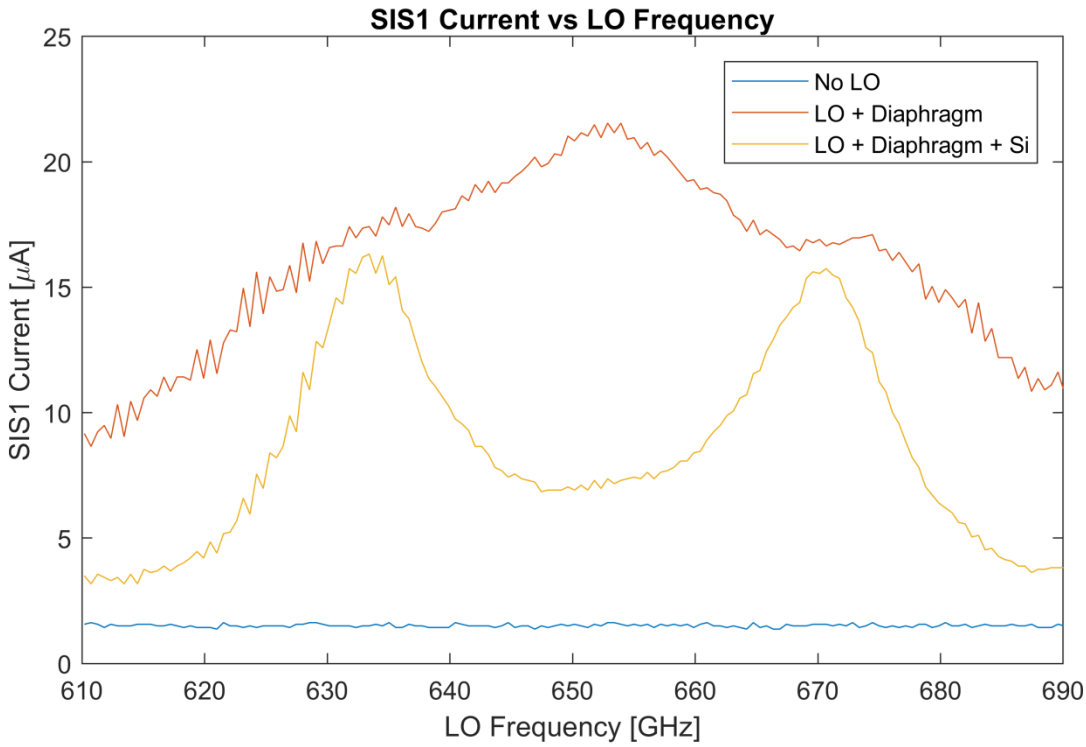

Figure 37: SIS bias current as a function of LO frequency. Notably, there are standing waves present due to the installation of a Si substrate leading to the two transmission peaks.

5.2 Blue LED

Now that the basic settings of the experiment have been detailed, first measurements with a light source could be carried out. The first measurements have been done with two high power blue LEDs ($I_{in} = 1A$) which were stitched together in series for maximum output power. First of all, the right LO frequency needs to be chosen for maximum THz transmission. This has been done before each of the measurements that were carried out. In order to do so, a plot has been made relating the SIS bias current to the LO frequency. In this case, the first Si transmission peak corresponds to a LO frequency of $f_{LO} = 644\ GHz$ as can be observed in the figure below (figure 38).

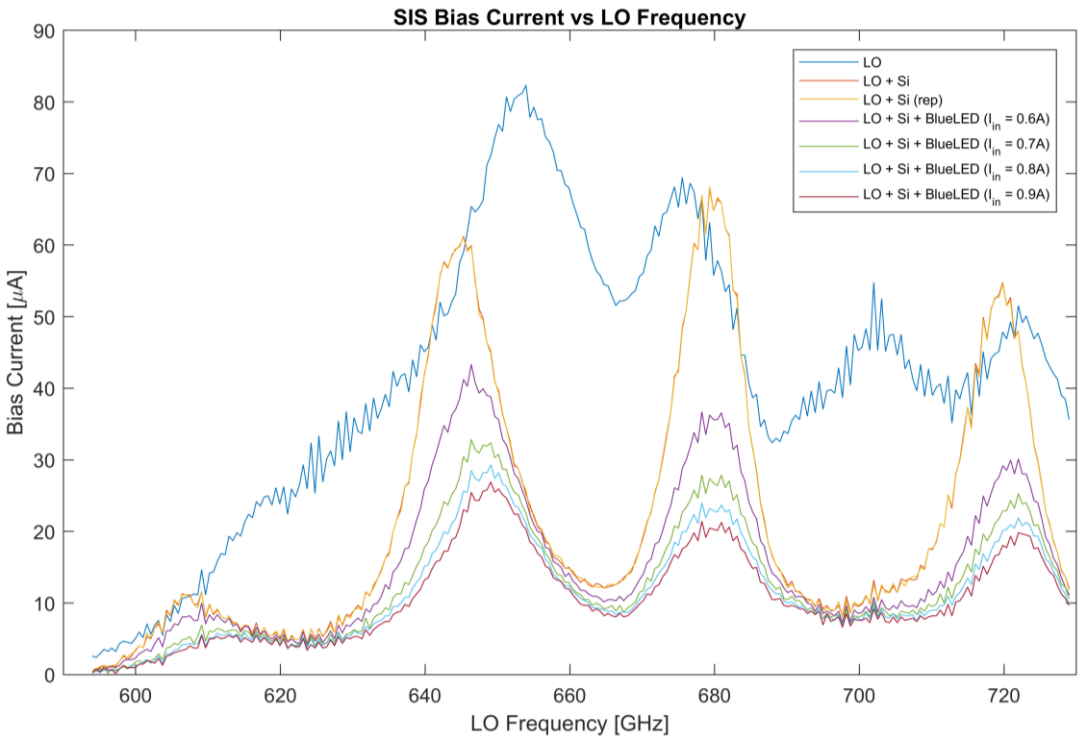

Figure 38: SIS bias current versus LO frequency using different illumination states of the blue LEDs. The LO frequency has been adjusted to the first Si transmission peak i.e. $f_{LO} = 644\ GHz$.

Noticeably, at some frequencies the Si peak is higher than the initial power of the LO signal which is due to refocussing of the Si peak. In order to properly compare the results with future measurements a normalisation has been applied together with a fudge factor. Hence, all results have been normalised with respect to the LO signal yielding the transmission and subsequently a fudge factor has been applied. The results have been depicted in figure 39.

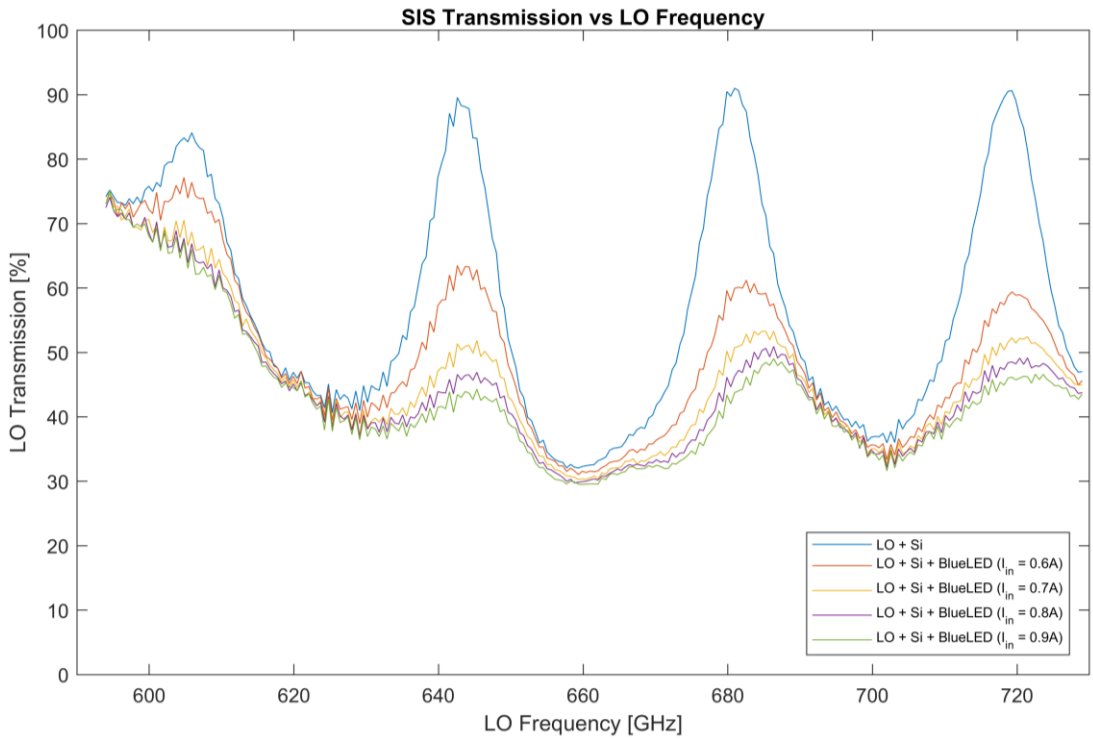

Figure 39: LO transmission relative to the initial LO power versus LO Frequency. Note that a fudge factor has been applied for future comparison of the results.

As can be observed from the graphs the maximum transmission with the Si substrate installed is in the order of 90%. The 10% loss corresponds predominantly to losses inside the Si substrate itself. The losses at the troughs mostly correspond to reflections of the THz beam from Si substrate (i.e. standing waves) as an electron plasma has been induced due to illumination with the two blue LEDs. Furthermore, the attenuation profile seems to be rather non-linear i.e. for discrete steps of input current, the attenuation becomes less prominent. Ultimately, with almost full illumination power, the transmission is slightly more than half of the initial Si transmission peak (around $40\ \%$). This would be a sufficient attenuation in order to analyse the noise temperature characteristics.

Subsequently, a measurement could be performed concerning the output power of intermediate frequencies (IF) from the SIS mixer versus grid motor angle. In essence, the grid consists of a small grating structure so that vertically polarised radiation will be transmitted. Since the radiation from the LO is vertically polarised, rotation of the grid will result in variation of the output power for the IF signal. This experiment has been carried out using two different temperature loads. A bucket of liquid nitrogen was installed together with a chopper so that the temperature could be changed alternately between 300K (hot load) and 77K (cold load). Hence, two curves have been made relating the IF power to the grid motor angle. The grid angle has been varied from $0 - 100°$ in steps of $0.25°$. See figure 40 for the results.

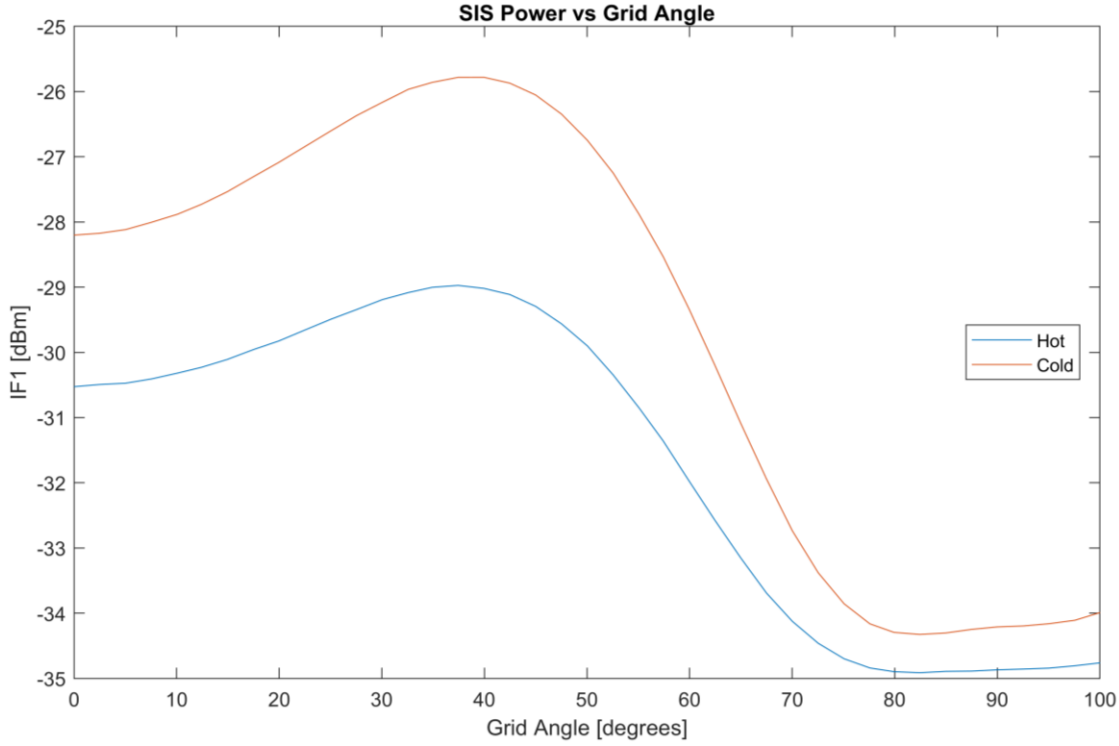

Figure 40: IF power versus grid rotation angle using a hot-cold source ($T_h = 300K$ and $T_c = 77K$ respectively).

Note that only the dark measurement has been taken as this is decisive for the optimal grid angle to be installed later on. Subsequently, the Y-factor can be computed which essentially is the hot-cold contrast. Since the IF power is defined in logarithmic units $[dBm]$, the Y-factor is simply the difference between the hot and cold load:

$$\boldsymbol{Y_{lin}} = \frac{\boldsymbol{P_{hot}}}{\boldsymbol{P_{cold}}}. \tag{33}$$

$$\boldsymbol{Y_{log}} = \boldsymbol{P_{hot}} - \boldsymbol{P_{cold}}. \tag{34}$$

The corresponding plot of the logarithmic Y-factor versus grid angle is shown in figure 41. As can be observed, hence an optimal grid angle of $\theta = 43°$ has been used.

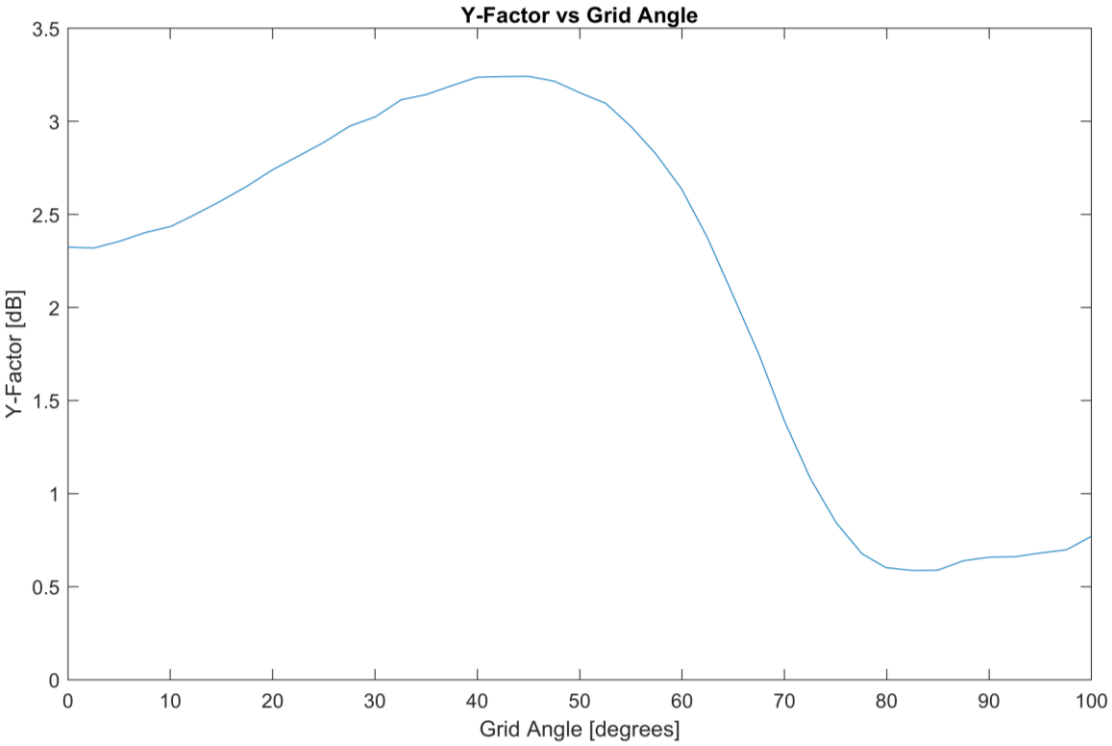

Figure 41: Logarithmic Y-factor versus grid angle for the dark measurement in case of the blue LED experiment.

Subsequently, measurements could be performed relating the yttrium-iron garnet (YIG) filter frequencies with IF power at the optimal grid angle (highest Y-factor). Essentially, the YIG filter is a bandpass filter in the range of $3 - 13\ GHz$ which is placed at room temperature outside of the $4K$ cryostat which contains the SIS mixer. Hence, the YIG filter will only transmit the IF frequencies that are of interest and specifically the $4 - 12\ GHz$ range has been used which is most applicable for ALMA. See figure 42 for the results.

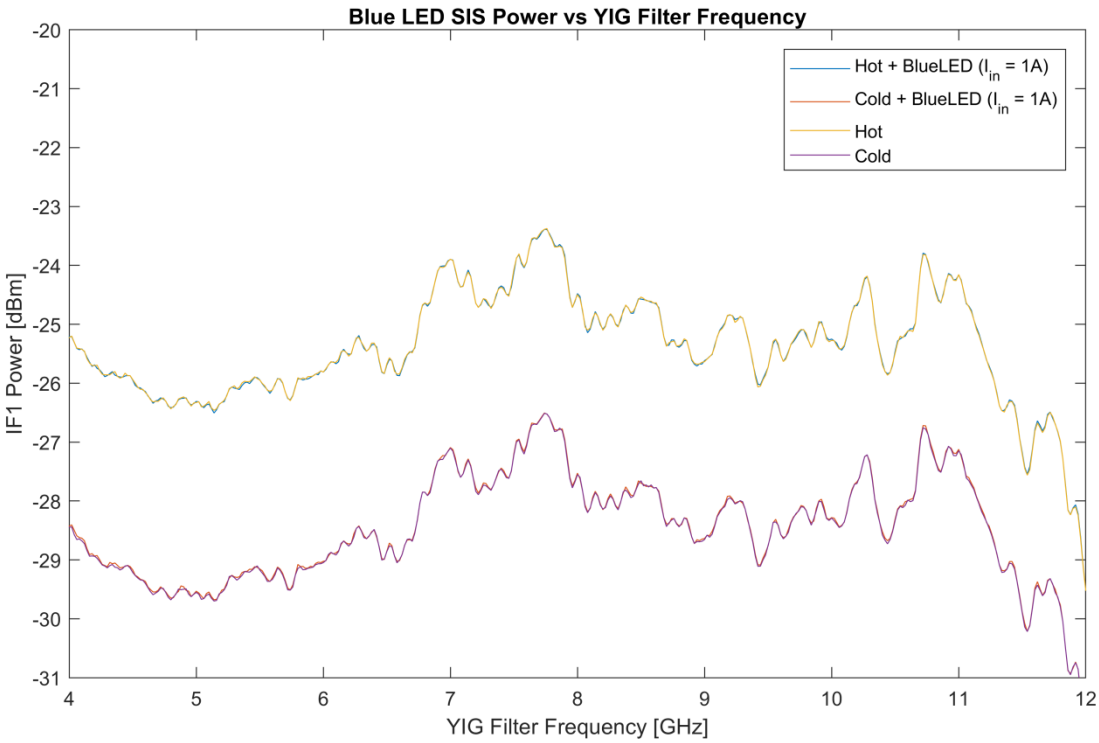

Figure 42: IF power versus YIG filter frequency for the dark-light measurement using a blue LED together with a hot-cold temperature load.

Remarkably, there is almost no difference present between the dark-light measurements.in the frequency range of interest. Predominantly, the hot-cold measurement shows a difference in the order of less than one dBm. Evidently, even with THz attenuation from the blue LEDs in the order of -5 dB, no significant difference in IF power is present. In order to make more rigorous statements, the system noise temperature should be computed which can be derived from the (linear) Y-factor as follows:

$$\boldsymbol{T_{sys}} = \frac{\boldsymbol{T_{hot} - YT_{cold}}}{\boldsymbol{(Y-1)}} = \frac{\boldsymbol{300-77Y}}{\boldsymbol{(Y-1)}}. \tag{35}$$

Subsequently, the system noise temperatures of the dark-light measurement could be related to the YIG filter frequency yielding the final plot regarding the blue LED experiment (see figure 43).

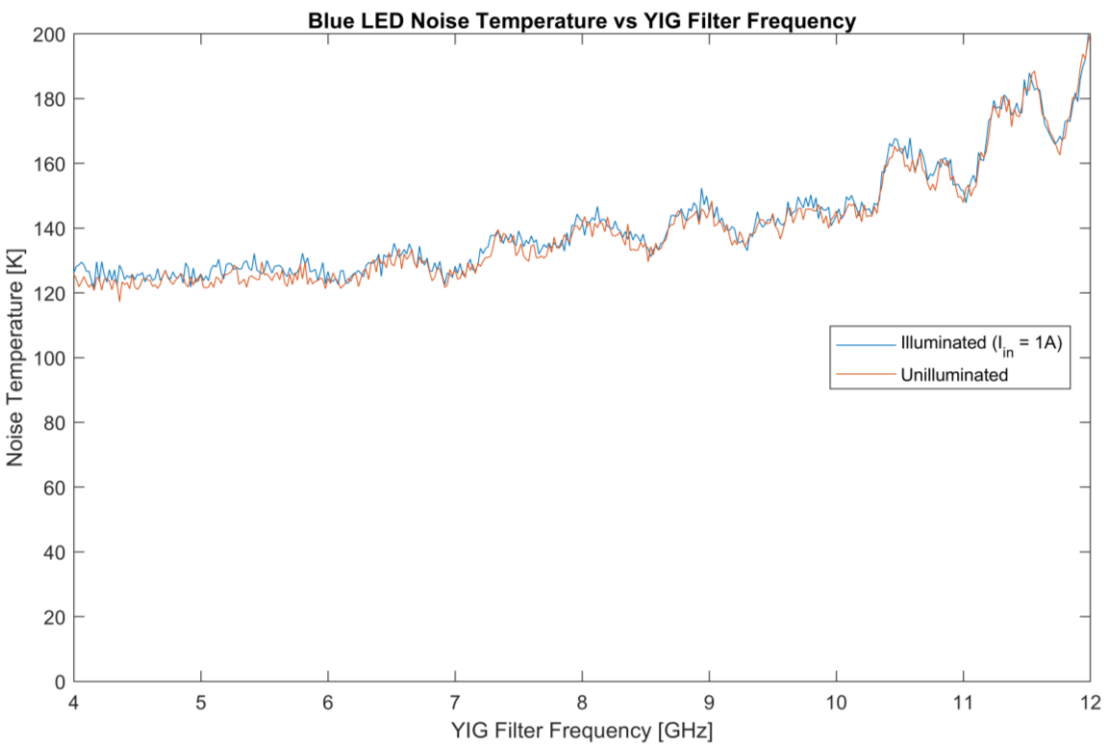

Figure 43: System noise temperature versus YIG filter frequency for the dark-light measurement using optical illumination of the Si substrate with two blue LEDs.

According to the results, the noise temperature does not vary significantly over the frequency range of the YIG filter which is most significant for ALMA. Hence, the results demonstrate that modulation of a THz beam with optical illumination of a Si substrate using the blue LEDs does not contribute significantly to the overall noise temperature. However, the fact that the difference in system noise temperature is this small could also be due to the relatively low THz attenuation of the blue LEDs. Another significant aspect is whether there could be a wavelength dependence of the noise temperature as an LED emits has a relatively narrow radiation spectrum. Hence, there is a need to investigate with different light sources and therefore similar measurements will be carried out with the microscope light as well as the halogen lamp. This will be detailed in the subsequent sections.

5.3 Microscope Light

In this section, the results for the heterodyne receiver experiment with the microscope light will be discussed. Similar to the blue LED measurements, the generation frequency has been optimised after the installation of the Si substrate corresponding to the first Si transmission peak i.e. $f_{LO} = 644\ GHz$. In fact, the microscope light measurements were performed sequentially to the blue LED measurements. In figure 44, the results are shown for the plot relating the SIS bias current to the LO frequency. Note that the same LO power has been used with a bias voltage $V_{bias} = 2\ mV$.

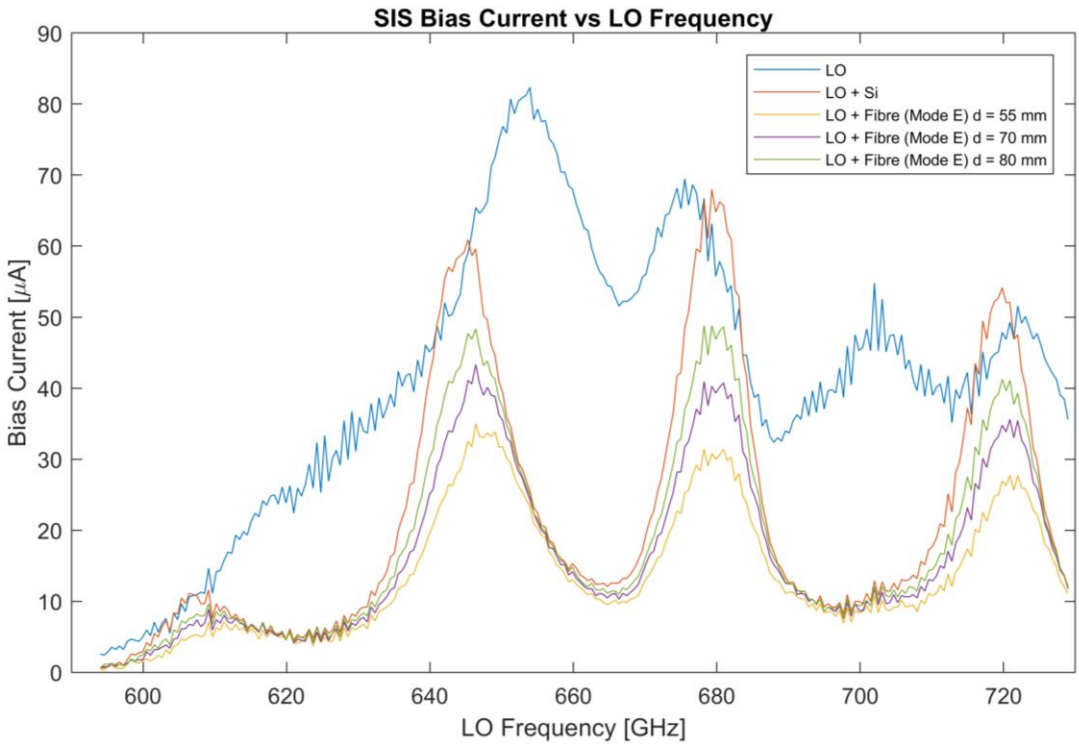

Figure 44: SIS bias current versus LO frequency using different illumination states of the microscope light (white light source). Similarly, the LO frequency has been adjusted to the first Si transmission peak i.e. $f_{LO} = 644\ GHz$.

The microscope light includes various illumination modes ranging from mode A (weakest) to mode E (strongest) and each mode has a slightly different radiation spectrum i.e. mode A is more yellow as compared to mode E. Mode E illumination has been chosen in combination with a hyperbolic lens with a short focal length as in this case the attenuation can be controlled more accurately. Similar to the blue LED measurements, a normalisation together with a fudge factor has been applied in order to review the results in a decent way This leads to another graph relating the LO transmission to the LO frequency as depicted in figure 45.

.

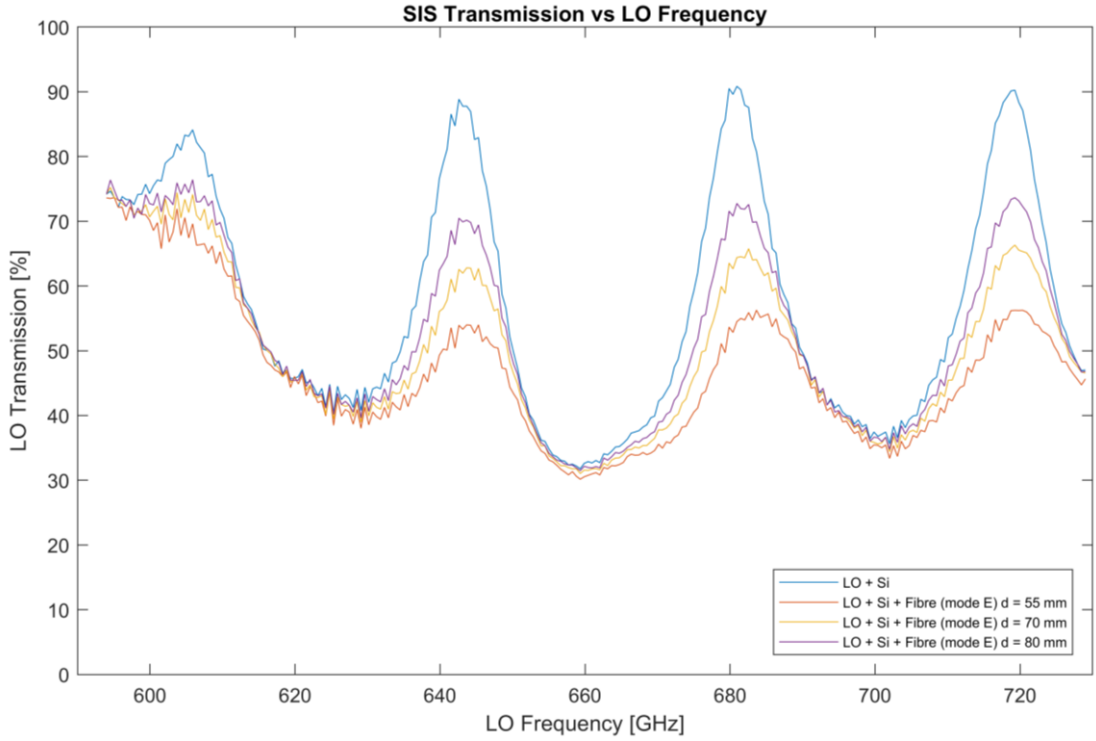

Figure 45: LO transmission relative to the initial LO power versus LO frequency in case of the heterodyne receiver experiment involving a microscope light. Similarly, a fudge factor has been applied in order to make a proper comparison of the results among the experiments.

As can be observed, the Si transmission peaks are equal in magnitude as in case of the blue LED experiment. In essence, the optical fibre of the microscope light has been moved away from the lens in discrete steps ($d = 55\,mm$, $70\,mm$ and $80\,mm$ respectively) yielding different illuminations with the same radiation spectrum. Remarkably, there seems to be a slight shift of the transmission peak to the right under optical illumination of the Si substrate. The shift is slightly more prominent than in case of the blue LED measurements. There could be various physical explanations for this phenomenon. Firstly, the shift could happen due to a temperature effect which could change the properties of the Si substrate such as thickness due to the expansion coefficient of Si. An experiment to study the heating effect will be carried out later on involving a heat gun and is described in a subsequent section. Secondly, there could be a change in relative permittivity of the Si substrate due to the electron plasma that was induced by the microscope light. This could be accurately tested by means of a high-resonance cavity to be studied in future experiments.

Subsequently, measurements could be carried out relating the IF power to the YIG filter frequency at the optimal grid angle corresponding to the highest Y-factor. Similar to the blue LED experiment, the YIG filter range has been set from $4 - 12\ GHz$, which is most applicable for ALMA. See figure 46 for the results.

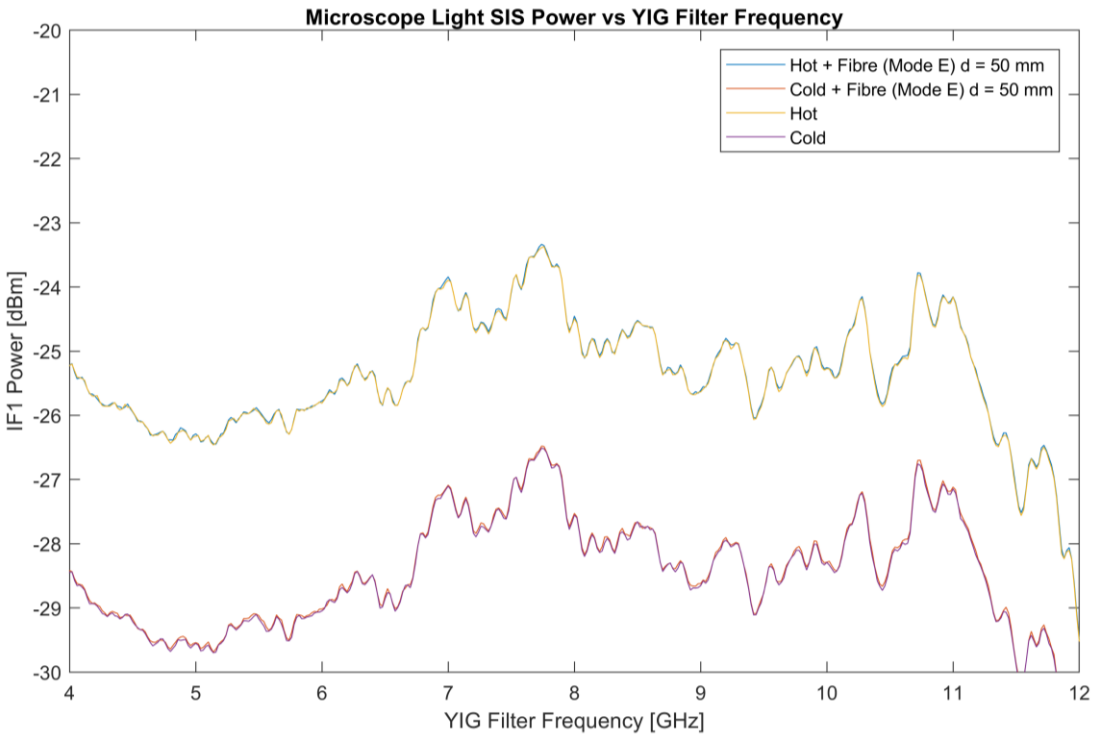

Figure 46: SIS power vs YIG filter frequency in case of the heterodyne receiver experiment involving the microscope light.

Also in this case there seems to be minimal changes in terms of IF power present which are in the order of less than $1\ dBm$. The highest illumination mode has been used with a distance of $d = 50\ mm$ to the lens for both the hot- and cold load. The magnitude difference in IF power between the hot-cold load measurements is similar to the results as was carried out with the two blue LEDs. Similarly, the Y-factor has been computed using the contrast between the IF powers for the dark-light measurements and subsequently the system noise temperature T_{sys} could be derived. This leads to the plot as illustrated in figure 47.

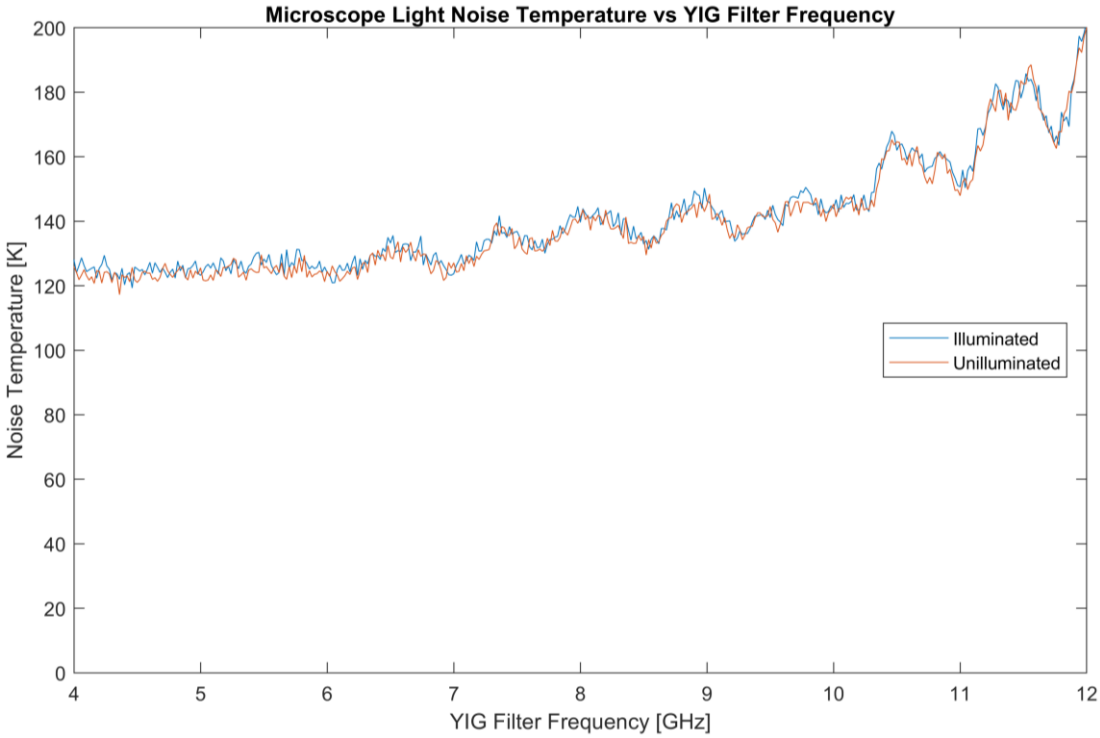

Figure 47: System noise temperature versus YIG filter frequency for the dark-light measurement using optical illumination of the Si substrate with the microscope light (halogen lamp with optical fibre).

Despite the relatively high THz attenuation of the microscope light (mode E illumination) in the order of $-15\ dB$, the contribution to the system noise temperature seems to be small as well. All in all, the results from this graph demonstrate that significant attenuation of a THz signal is possible using the microscope light with minimal contributions to the noise temperature. In order to investigate whether these results are consistent or merely coincidence, measurements will be performed with another white light source namely with a halogen lamp. The results for these measurements will be outlined in the next section.

5.4 Halogen Lamp

In this section, the results for the heterodyne receiver experiment with optical illumination of a Si substrate using a halogen lamp will be discussed. The optical scheme is the same as was the case for the FTS experiment, including an internal reflector as well as a hyperbolic lens. The first measurement that was carried out is concerned with the IF power related to the grid rotation angle (see figure 48). For the dark measurement, the grid angle was varied from $30 - 60°$ in steps of $0.25°$ whereas for the light measurement the grid angle was varied from $0 - 60°$ in steps of $0.5°$. The motive for these range settings is that the illuminated curves are much flatter and wider than the unilluminated curve. This result might have to do with either a heating effect of the Si substrate or the wide radiation spectrum (white light) of the halogen lamp.

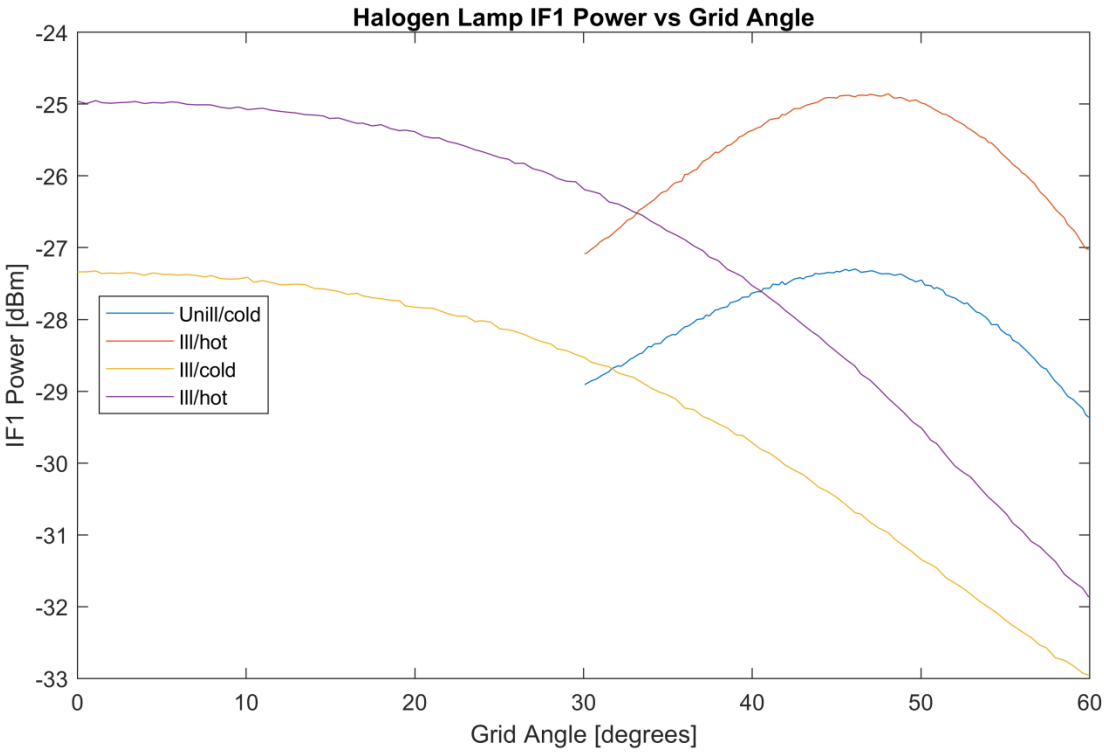

Figure 48: IF power versus grid rotation angle using illumination of the Si substrate with a halogen lamp together with a hot-cold load.

From the IF power curves, the corresponding logarithmic Y-factors were computed for both the unilluminated and illuminated case. This leads to the graph in figure 49. Interestingly, the illuminated Y-factor seemed to be flattened and shifted with respect to the grid angle. Similarly, the peak of the unilluminated Y-factor has been chosen for the optimal grid angle i.e. $\theta = 50°$.

Figure 49: Y-factor versus grid rotation angle for the dark-light measurement with the halogen lamp.

Using the optimal grid angle of the unilluminated curve ($\theta = 50°$), the measurement relating IF power to the YIG filter frequency could be carried out. Similar settings as in previous measurements have been used i.e. a YIG frequency range of $3 - 13\ GHz$. See below for the results (figure 50).

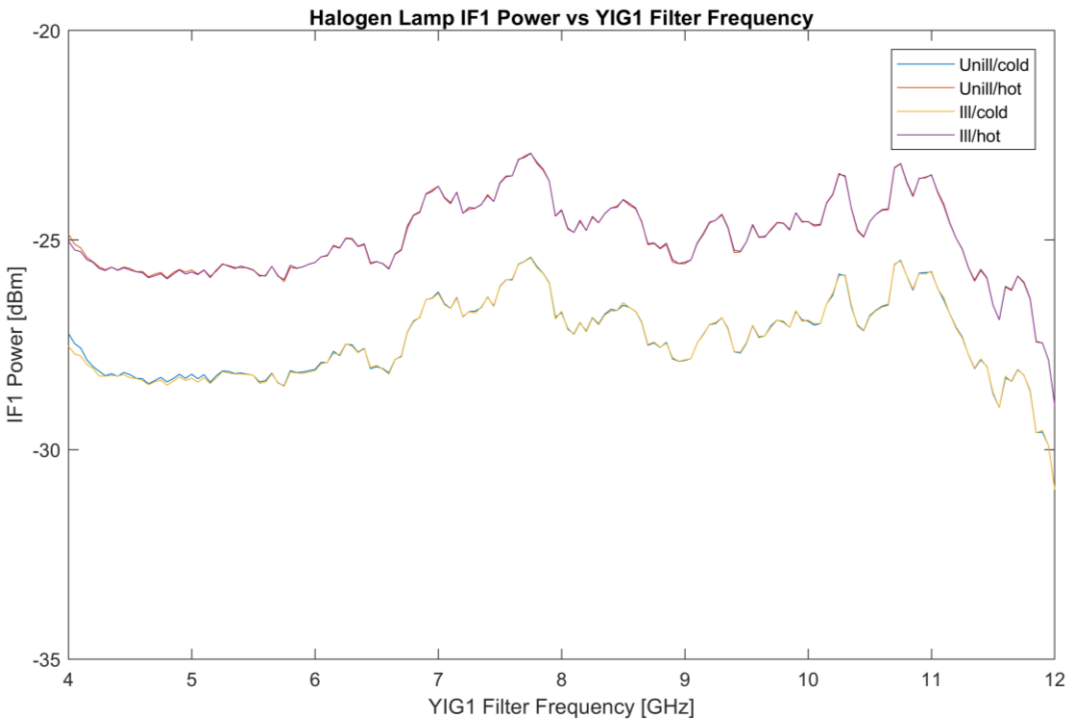

Figure 50: IF power versus YIG filter frequency by optical illumination of the Si substrate with a halogen lamp in conjunction with a hot-cold source.

As can be observed from the figure, there is no major difference present between the dark-light measurements. Around $4\ GHz$ there seems to be a slight bump in the order of $1-2\ dBm$ but this is not too significant. The magnitude of the IF power is comparable to the previous measurements carried out with the blue LEDs and the microscope light. Similarly, to derive the system noise temperature, the corresponding (linear) Y-factors were computed from the IF power curves .This resulted in a plot relating noise temperature versus YIG frequency as illustrated below in figure 51.

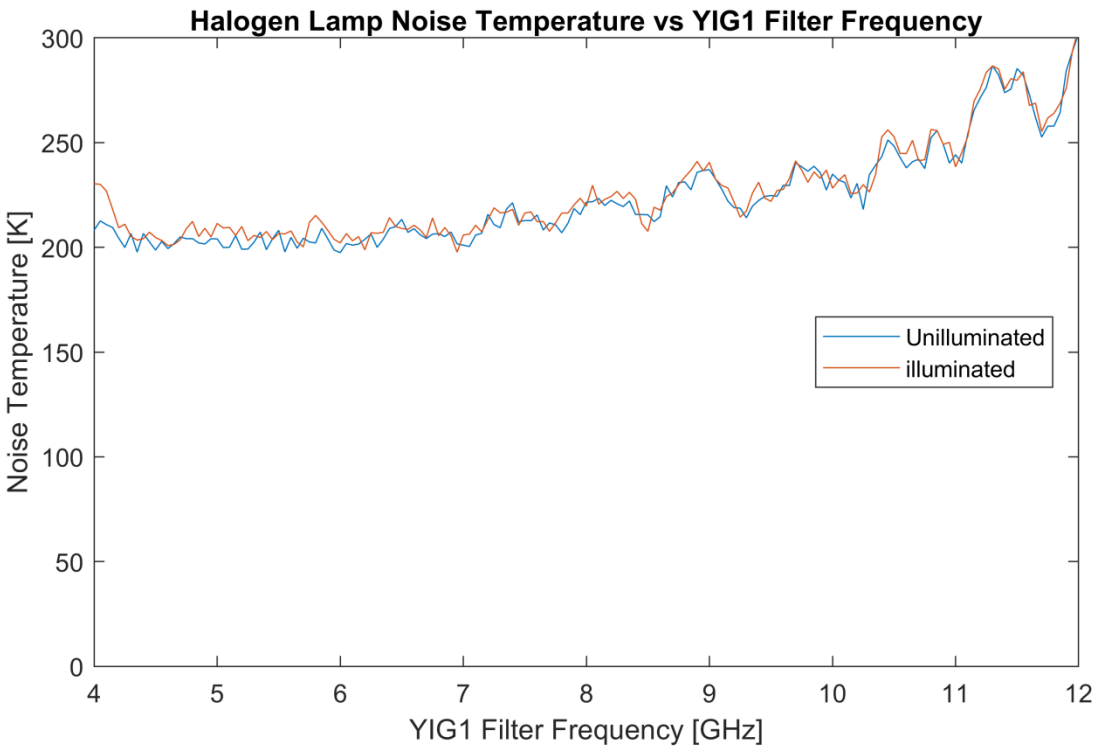

Figure 51: System noise temperature versus YIG filter frequency for measurements with the halogen lamp. .

Remarkably, it appears that the curve related to the light measurement is somewhat higher in noise temperature up to frequencies of $4.5\ GHz$.For the rest of the frequency range, the two curves coincide rather well with minor differences present. Hence, also illumination of the Si substrate with a halogen lamp does not seem to significantly contribute to the noise temperature of the heterodyne receiver. So up until now, optical illumination of the Si substrate with three different light sources to modulate the THz beam does not appear to considerably modify the overall system noise temperature. Another feature that is of significant interest is concerned with the phase noise present in the central IF signal i.e. $|f_1 - f_2|$. The results for these measurements require a slightly different setup and will be detailed in the section 5.6. In the subsequent section, the heating effect of the Si substrate will be investigated.

5.5 Heat gun

In order to investigate the heating effect of silicon in more detail, measurements have been carried out involving a heat gun. The predominant feature that has been measured is whether there is an effect in terms of transmission present. Hence, first of all a plot has been made relating the SIS bias current to the LO frequency. The grid angle has been set to $\theta = 45°$ which corresponds to the maximum Y-factor. See figure 52 for the corresponding plot.

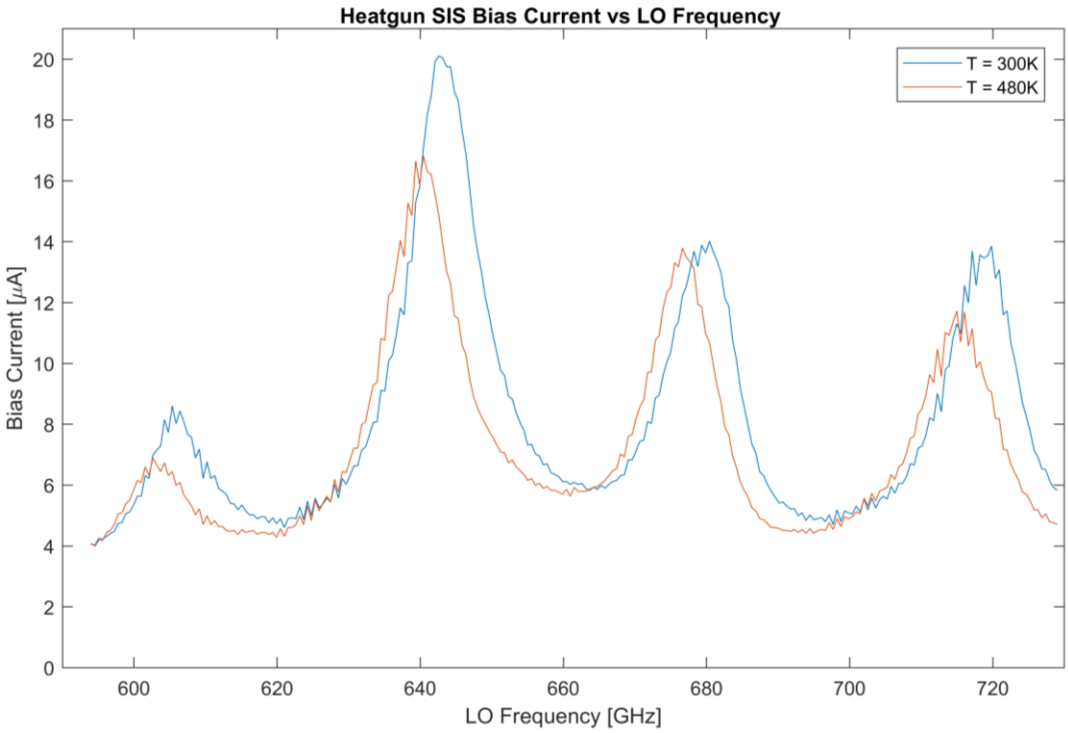

Figure 52: SIS bias current vs LO Frequency in case of the experiment involving a heat gun.

Remarkably, in this case the Si transmission peak seems to be shifted to the left as compared to illumination where the peak was shifted to the right. Clearly, the transmission peak is somewhat suppressed also which would imply that a heating effect can be rather significant. Hence, it is apparent that heating of the Si substrate induces charge carriers also which reflects part of the THz beam. Therefore, both the illumination itself as well as heating of the silicon contributes to modulation of the THz beam. However, it is rather difficult to precisely state which fraction is due to the heating effect and which fraction is due to illumination. Moreover, thermal expansion of the Si substrate could be part of the shift in transmission peak but would however be on the percentage level (Swenson, 1983). In all likelihood, taking a closer look at the results from previous measurements, attenuation of the THz beam using the microscope light as well as the halogen lamp would be attributed to the heating effect more than in case of the blue LED measurements.

5.6 Phase Noise Experiment

In this section, the results for the phase noise experiment will be discussed. Overall, the setup is similar to the heterodyne receiver experiment except that in this case the hot-cold load is replaced by another LO namely the test LO. An overview of the modified setup can be found in figure 53. The frequency of the test LO is tuned in such a way that the central frequency of the IF signal is $|f_{LO,test} - f_{LO,source}| = 6\ GHz$. Since the source LO is set to the frequency of the first Si transmission peak $f_{LO,source} = 643.95\ GHz$, the test LO is set to $f_{LO,test} = 649.95\ GHz$.

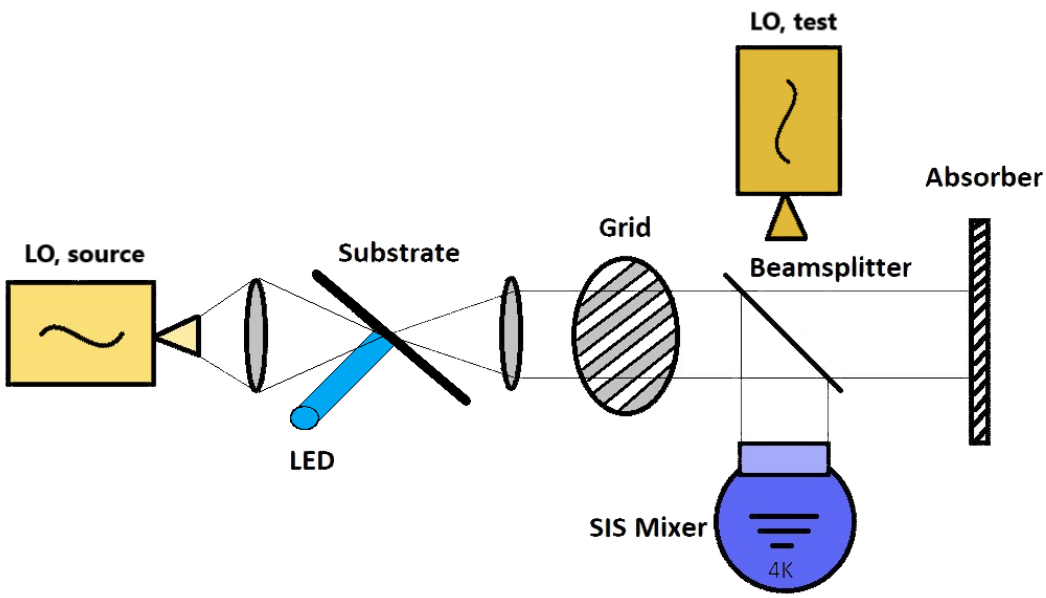

Figure 53: Overview of the modified setup for the heterodyne receiver experiment. Note that the source LO is set to $f_{LO,source} = 643.95\ GHz$ and the test LO is set to $f_{LO,test} = 649.95\ GHz$.

First of all, the optimal grid angle needs to be set for the test source which corresponds to the highest Y-factor and hence the lowest amount of noise temperature. Therefore, a corresponding plot has been made as shown in figure 54 below.

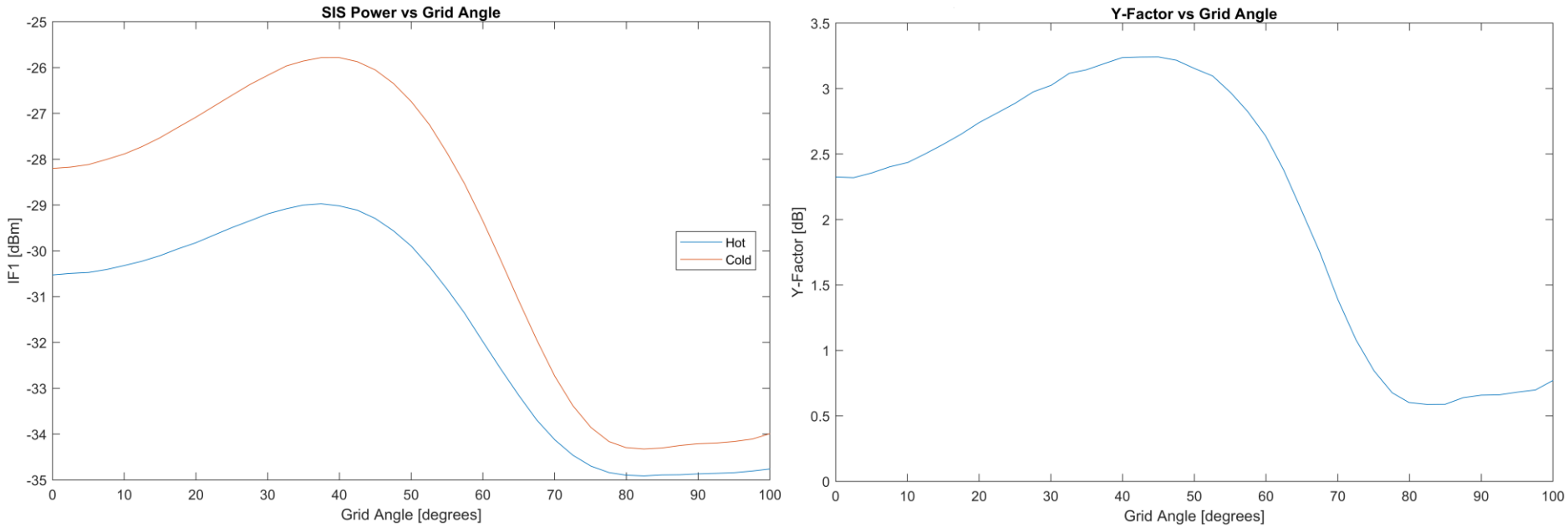

Figure 54: Plots relating the IF power to the grid angle leading to the maximum Y-factor. The optimal grid angle corresponding to this Y-factor is $\theta = 42.5°$.

In this experiment, three measurements have been performed namely two light measurements (Blue LEDs + microscope light) and a dark measurement. A spectrum analyser has been used to display the central IF frequency together with the phase noise. Twelve frequency scales have been used from $50\ MHz$ up to $100\ Hz$ containing different resolution bandwidths (RBW). Effectively, the RBW is the minimum separation of two frequency components that can still be distinguished. Correspondingly, double sideband plots have been constructed for six frequency scales in logarithmic steps from $10\ MHz$ up to $100\ Hz$. This selection was most convenient to acquire a quick overview whether noise features are present or not. The results have been illustrated in the figures below (figures 55-57). The power has been expressed in decibels relative to the carrier (dBc) i.e. relative to the central frequency peak. This implies that:

$$\boldsymbol{P[dBc] = 10\log_{10}\frac{P_{ph}}{P_c}}. \tag{36}$$

Here, P_{ph} is the phase noise power and P_c is the central power.

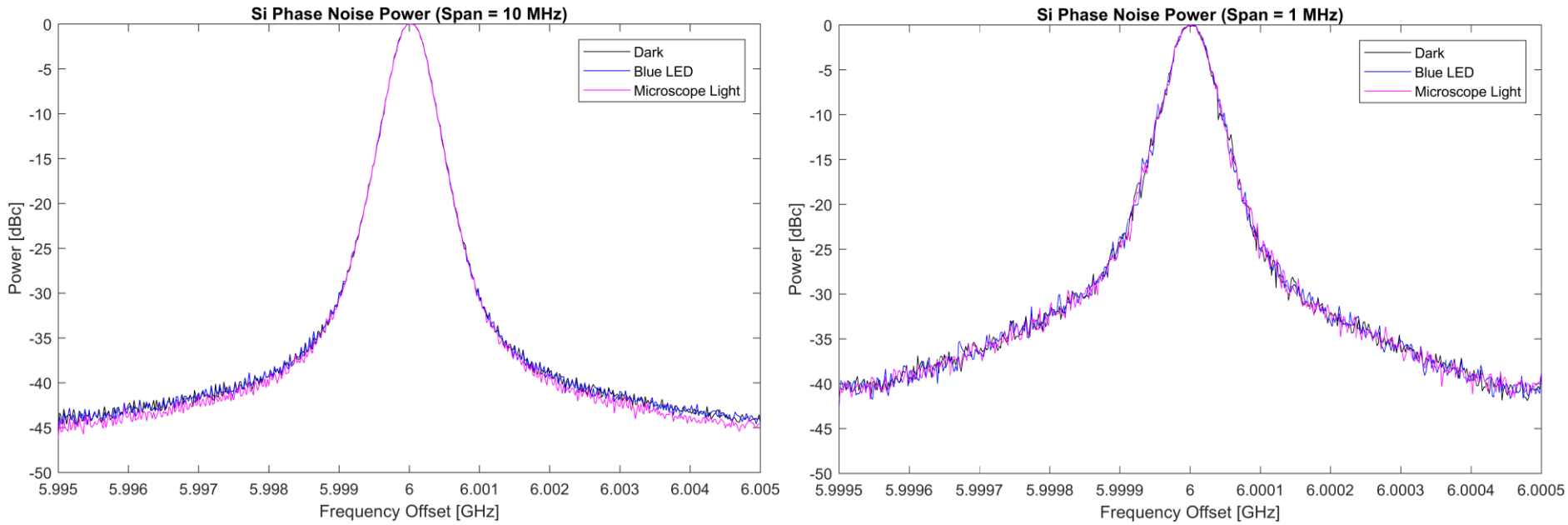

Figure 55: Noise Power vs central frequency using a source LO as well as a test LO operating at $f_{LO,test} = 649.95\ GHz$ and $f_{LO,source} = 643.95\ GHz$ respectively for the $10\ MHz$ and $1\ MHz$ span.

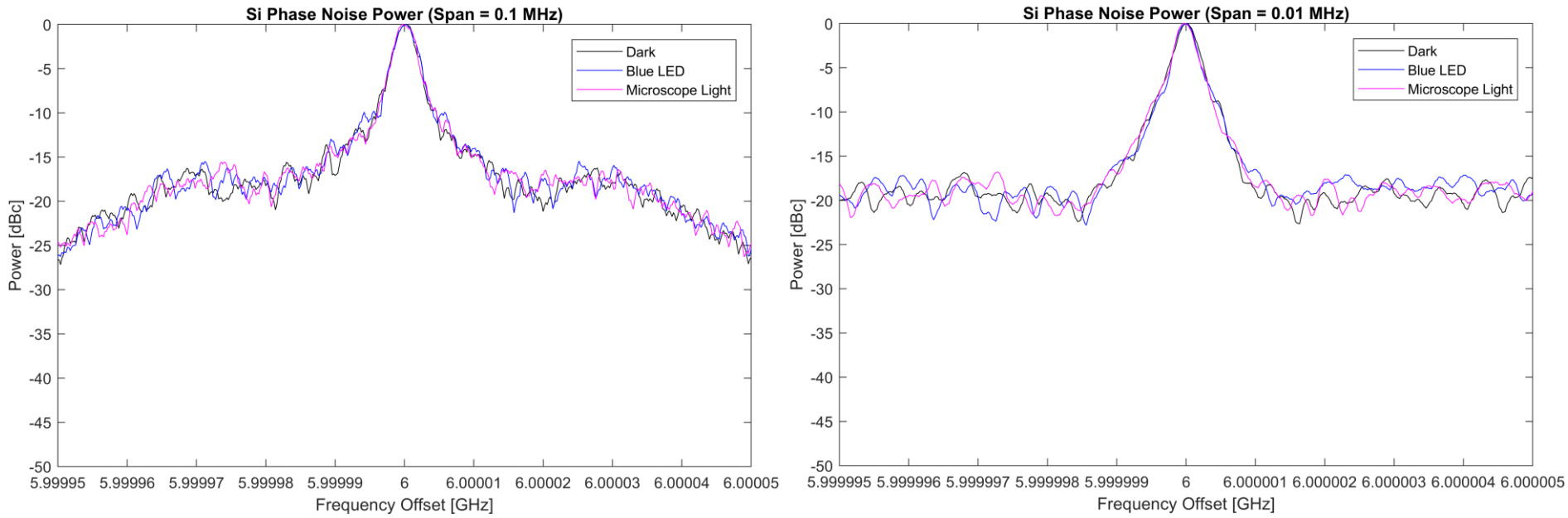

Figure 56: Noise Power vs central frequency using a source LO as well as a test LO operating at $f_{LO,test} = 649.95\ GHz$ and $f_{LO,source} = 643.95\ GHz$ respectively for the $0.1\ MHz$ and $0.01\ MHz$ span.

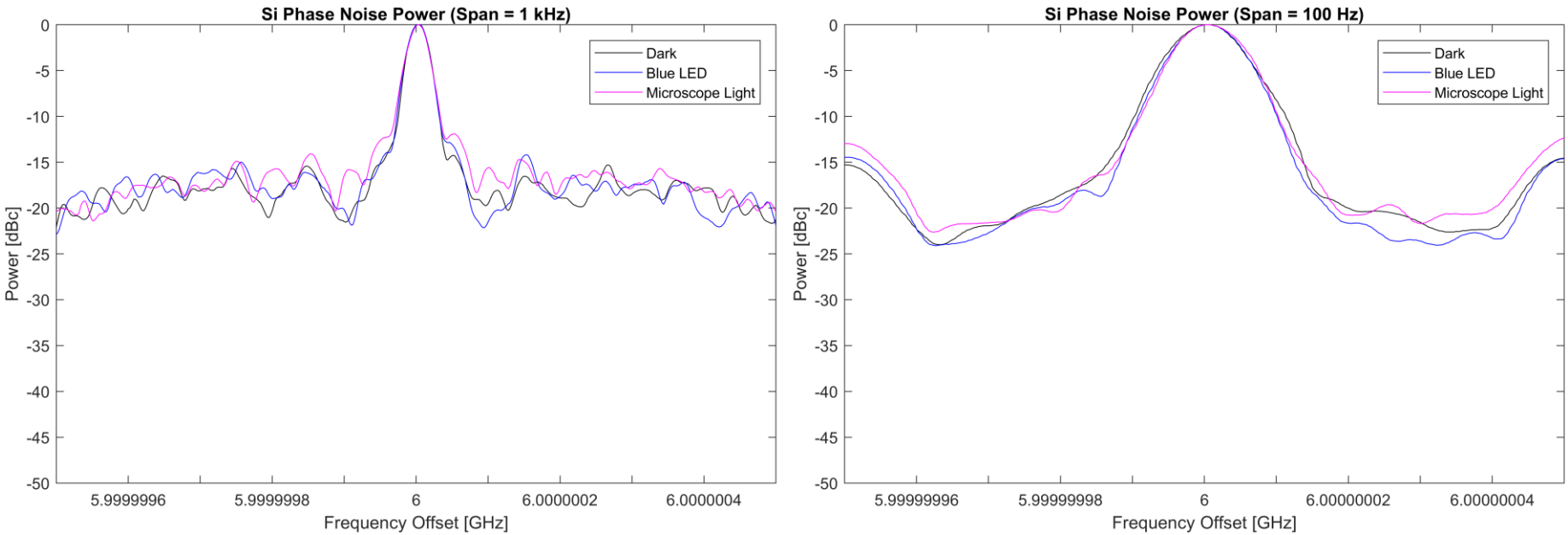

Figure 57: Noise Power vs central frequency using a source LO as well as a test LO operating at $f_{LO,test} = 649.95\ GHz$ and $f_{LO,source} = 643.95\ GHz$ respectively for the $1\ kHz$ and $100\ Hz$ span.

For the $10\ MHz - 0.1\ MHz$ spans, the amount of phase noise power present seems to be rather minimal. However, for the shorter frequency spans ($0.01\ MHz - 100\ Hz$) there appears to be certain differences. On the $0.01\ \&\ 1\ kHz$ scales, both the blue LED and microscope light measurements contribute to slightly more fluctuations in phase noise power than the dark measurement. At the $100\ Hz$ span there are also some differences present however still very minimal at first sight. Remarkably, the differences in phase noise power on the right sight of the carrier is somewhat higher as compared to the left side. Nonetheless, these values are still within a $\sim 5\ dBc$ limit which is not too significant.

In order to make a more detailed analysis, the single sideband phase noise plots have been constructed. The single sideband plots relate the power of the phase noise relative to the central power (dBc) at various frequency offsets. In this case all twelve frequency spans have been used as outlined before. Evidently, the RBW of the shortest span has been used and hence the power of all other spans were normalised to the $10\ Hz$ RBW. In this manner, the amount of power per frequency range is the same. Consequently, the amount of noise power is then defined in terms of $dBc/10\ Hz$. In essence, this implies the amount of noise power that is measured relative to the carrier in a $10\ Hz$ bandwidth centred at twelve frequency offsets from the carrier Moreover, the phase noise is symmetric with respect to the central frequency peak, so either the left or the right part of the central frequency peak can be chosen. In this case, the right part of the central frequency peak has been taken which was most convenient in terms of indexing i.e. stitching all twelve curves together. Consequently, a logarithmic plot could be constructed as depicted in figure 58.

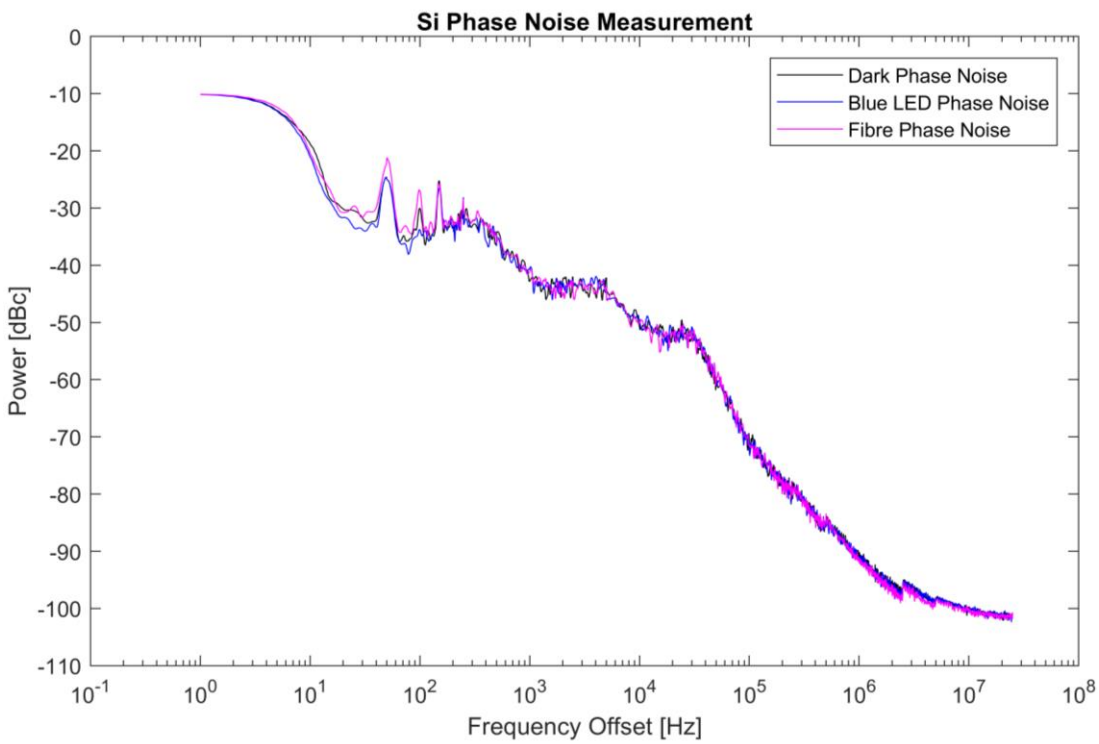

Figure 58: Phase noise power $[dBc]$ vs frequency offset $[Hz]$ for the dark- and light measurements including illumination with the blue LEDs as well as the microscope light.

Interestingly, at least up to the $10\ kHz$ scale there does not seem to be much of a difference in the amount of phase noise power present for all three measurements. Below the $10\ kHz$ span there are a couple of noise peaks present. In all likelihood, these peaks are due to (harmonics of) the mains hum i.e. at $50\ Hz$, $100\ Hz$ and $150\ Hz$. In case of ALMA, the noise present in the smaller frequency offset regime of the spectrum ($< 10\ kHz$) do not make a significant contribution as the frequency resolution of ALMA lies around $100\ kHz$. So the result as presented here reveals that modulation of the THz beam with various optical illuminations does not affect the amount of phase noise power in the frequency offsets of interest . This might be an important result considering possible implementation of a high resistivity Si substrate for THz modulation in the phased array feeds of ALMA.

6. Conclusions and Discussion

The experiments that have been carried out and which were detailed in this thesis revealed various results which are of significance for the ALMA project. First of all, the calibration experiment revealed that there is a modified inverse power law dependence present between the intensity of THz radiation and the intensity of optical illumination. This became evident in the measurement with the halogen lamp connected to an optical fibre were the lock-in voltage was related to the photodiode current. Furthermore, in the FTS experiment it became clear that within the accuracy of the measurement we could not conclude whether there was a change in relative permittivity observable, even for the high-resolution measurements. According to the intensity ratio plots, there is a frequency dependence present on THz transmission for high-resistivity Si. At lower frequencies there is more reflection and losses as compared to the higher frequencies. This result is consistent with all light sources that have been used in the experiments. This is a significant result as the LOs used in ALMA operate in the range of $600 - 750\ GHz$. Subsequently, in the heterodyne receiver experiment it was demonstrated that optical illumination of the Si substrate for all light sources does not contribute to the noise temperature present. In addition, up to the spectral resolution of ALMA $(100\ KHz)$ there is no added phase noise present in various frequency offsets from the central carrier wave due to optical illumination of the Si substrate.

Theoretically, the charge carrier lifetime turned out to be a crucial parameter as regards THz modulation. The lifetime changes for different semiconductor materials such as GaAs and Ge, therefore different amounts of irradiance of the substrate is required. In general, a high amount of irradiance is required to attenuate the THz beam for a Si substrate effectively i.e. in the order of $4.2\ W/cm^2$ to achieve a THz attenuation of $-35dB$ (Jiang et al., 2017). Interestingly, in the heterodyne receiver experiment the transmission peaks shift to the right due illumination whereas the transmission peaks shift to the left due to heating of Si with the heat gun. Moreover, it is not obvious which part of the attenuation is due to illumination and which part is due to heat. Hence, in order to investigate these findings further study is required in the future. Furthermore, future experiments could be carried out with different types of Si i.e. with anti-reflection coatings and other semiconductor materials such as GaAs and Ge could be of interest as well. Nonetheless, the method of optical illumination of a semiconductor substrate to modulate THz radiation as presented in this thesis is deemed suitable for use in a low noise heterodyne system. Therefore, the results will be a significant contribution considering the use of semiconductor materials in the phased array feeds of ALMA.

A. Green's Function for Two-Dimensional Carrier Concentrations

In case of the two-dimensional steady-state solution that satisfied the continuity equation (i.e. partial differential equation) of the photo-excited carrier concentration, a corresponding Green's function has to be constructed. The two-dimensional solution satisfies the boundary conditions at $z = 0$ and $z = h$ namely $\partial_z n(x,z)|_{z=0} = 0$ and $\partial_z n(x,z)|_{z=h} = 0$ and is defined as follows (Kannegulla, 2015):

$$\boldsymbol{N_e^{2D}(x,z) = \int_0^h \int_{\frac{-w}{2}}^{\frac{w}{2}} \frac{g(\eta)}{D_{eff}} G(x,z,\xi,\eta) d\xi d\eta} \ . \tag{37}$$

Here, $G(x,z,\xi,\eta)$ is the Green's function and $g(\eta) = \alpha P_0 (1-R) e^{-\alpha\eta/h\nu}$ is the carrier generation rate. Hence, the corresponding Green's function is given by (Kannegulla, 2015):

$$\boldsymbol{G(x,z,\xi,\eta) = \frac{1}{2\pi} \sum_{n=-\infty}^{\infty} \left[K_0 \left(\frac{\sqrt{(x-\xi)^2 + [z-(2nh+\eta)]^2}}{L_D} \right) + K_0 \left(\frac{\sqrt{(x-\xi)^2 + [z-(2nh-\eta)]^2}}{L_D} \right) \right]} . \tag{38}$$

The Green's function is defined in terms of the modified Bessel function of the second kind K_0 and is a function of the carrier diffusion length $L_D = \sqrt{\tau_e D_{eff}}$. Let $\beta = \sqrt{(x-\xi)^2 + [z-(2nh+\eta)]^2}/L_D$, then for the special case of $n' = 0$ the modified Bessel function becomes (Weisstein, 2018):

$$\boldsymbol{K_0(\beta) = \int_0^\infty \cos(\beta \sinh t)\, dt = \int_0^\infty \frac{\cos(\beta t)}{\sqrt{t^2+1}} dt} . \tag{39}$$

Consequently, this result can be substituted into the equation defining the Green's function yielding the following final expression:

$$\boldsymbol{G(x,z,\beta,\beta') = \frac{1}{2\pi} \sum_{n=-\infty}^{\infty} \left[\int_0^\infty \frac{\cos(\beta t) + \cos(\beta' t)}{\sqrt{t^2+1}} dt \right]} . \tag{40}$$

, with β as described previously and $\beta' = \sqrt{(x-\xi)^2 + [z-(2nh-\eta)]^2}/L_D$.

7. Bibliography

Baryshev Andrey Front-end Detectors for the Submm [Book Section] // Basic Detection Techniques. - Groningen : SRON, 2015.

Benford D.J., Kooi J.W. and Serabyn E. Spectroscopic measurements of optical components around 1 terahertz [Book Section]. - [s.l.] : California Institute of Technology, 1998.

Born M. and Wolf E. Principles of Optics [Book]. - [s.l.] : Cambridge University, 1999.

Dickmann Fabry Perot Resonator [Book Section]. - Eschbach : Fachhochschule Münster, 2003.

Dunleavy L. S-parameters [Book Section]. - [s.l.] : University of South Florida.

Gallacher T. Optoelectronic Modulation of mm-Wave Beams using a Photo-Injected Semiconductor Substrate [Book Section]. - St Andrews : [s.n.], 2012.

Graham James R. Convolution, Correlation & Fourier Transforms [Book Section]. - 2009.

Hecht E. Optics [Book Section]. - [s.l.] : Pearson, 2017. - Fifth.

Jarry P. and Beneat J. Scattering Parameters and ABCD Matrices [Book Section]. - 2008.

Jiang et al. A 740-GHz Dynamic Two-Dimensional Beam-Steering and Forming Antenna Based on Photo-Induced Reconfigurable Fresnel Zone Plates [Journal]. - [s.l.] : IEEE TRANSACTIONS ON TERAHERTZ SCIENCE AND TECHNOLOGY, 2017. - VOL. 7, NO. 3 : Vol. MAY 2017.

Kannegulla Akash et al. Photo-induced Spatial Modulation of THz Waves: Opportunities and Limitations [Journal]. - [s.l.] : Optical Society of America, 2015. - 25 : Vol. 23.

Liu Xiang Fourier Transform Interferometer [Journal]. - 2012.

Lumileds Luxeon Z Color Line [Book Section]. - United States : [s.n.], 2017.

MIT Lecture 11: Basic Josephson Junctions [Journal]. - [s.l.] : Massachusetts Institute of Technology, 2003.

NIST The NIST Reference on Constants, Units and Uncertainty [Online] // Base unit definitions_ Candela. - International System of Units (SI), 1979. - https://physics.nist.gov/cuu/Units/candela.html.

Palik E.D. Handbook of Optical Constants of Solids [Book]. - [s.l.] : Academia, 1988.

Parnell W.J. Green's Functions, integral equations and applications [Book Section] // Green's functions in 2 and 3D. - 2013.

Swenson C.A. Recommended Values for the Thermal Expansivity of Silicon from 0 to 1000 K [Book Section]. - [s.l.] : Phys. Chem. Ref., 1983. - Vol. 12.

Thorne Anne P. Spectrophysics [Book Section]. - New York : Chapman and Hall, 1988.

Tucker John R. and Feldman Marc J. Quantum Detection at Millimiter Wavelengths [Book Section]. - [s.l.] : Rev.Mod.Phys, 1985.

Ulbricht R. [et al.] Carrier dynamics in semiconductors studied with time-resolved terahertz spectroscopy [Journal]. - [s.l.] : Reviews of Modern Physics, 2011. - Vol. 83.

University of Reading Absorption and Extinction Coefficient Theory [Online]. - 2018. - http://www.reading.ac.uk/ir-substrateopticaltheory-absorptionandextinctioncoefficienttheory.aspx.

Vishay Silicon Photodiode BPW21R // Vishay Semiconductors. - February 2017.

Weisstein Eric Michelson Interferometry [Online] // Fourier Transform Spectrometer. - Wolfram Research, 2007. - http://scienceworld.wolfram.com/physics/FourierTransformSpectrometer.html.

Weisstein Eric W. Modified Bessel Function of the Second Kind. [Online] // MathWorld--A Wolfram Web Resource. - 2018. - http://mathworld.wolfram.com/ModifiedBesselFunctionoftheSecondKind.html.